Article

Effect of Sc:Zr Ratio on Superplastic Behavior of Ultrafine-grained Al-6%Mg-Sc-Zr Alloys

V.N. Chuvil'deev, M.Yu. Gryaznov, S.V. Shotin, A.V. Nokhrin *, C.V. Likhnitskii, G.S. Nagicheva, M.K. Chegurov, V.I. Kopylov, O.P. Pirozhnikova, A.A. Bobrov

Materials Science Department, Physical and Technical Research Institute, Lobachevsky State University of Nizhny Novgorod, 603022, Nizhny Novgorod, Russia; chuvildeev@nifti.unn.ru (V.C.); gryaznov@nifti.unn.ru (M.G.); shotin@nifti.unn.ru (S.S.); nokhrin@nifti.unn.ru (A.N.); likhnitskiy@nifti.unn.ru (C.L.); nagicheva@nifti.unn.ru (G.N.); yashadrina@nifti.unn.ru (I.S.); mkchegurov@nifti.unn.ru (M.C.); bobrov@nifti.unn.ru (A.B.); kopylov@nifti.unn.ru (V.K.); pirozhnikova@nifti.unn.ru (O.P.).

* Correspondence: nokhrin@nifti.unn.ru (A.N.)

Abstract: Al-6%Mg-Sc-Zr alloys with the total ratio of Sc + Zr = 0.32 wt.% make up the target of this research. The content of scandium and zirconium varied with an increment of 0.02%. The alloys were produced by induction casting. Their ultrafine-grained (UFG) microstructure was formed with Equal Channel Angular Pressing (ECAP). Such cast alloys have a homogeneous macrostructure formed by small equiaxed grains in the central part of the ingot and columnar crystals along the edges of the cross section. After ECAP, the average grain size in the alloy specimens is 0.5–1 μm. The average grain size does not depend on the ratio of Sc and Zr in these alloys. Superplasticity tests were performed at temperatures ranging from 300 to 500 °C and at a strain rate varying between $3.3 \cdot 10^{-3}$ and $3.3 \cdot 10^{-1}$ s^{-1}. UFG Al-6%Mg-0.20%Sc-0.12%Zr and Al-6%Mg-0.18%Sc-0.14%Zr alloys exhibit the highest superplasticity. It was suggested that changes in Sc:Zr ratio affect spatial distribution and composition of the following precipitating particles: Al_3Sc, Al_3Zr, $Al_3(Sc_xZr_{1-x})$. An increase in Zr concentration is shown to reduce the susceptibility of UFG alloys to cavitation fracture.

Keywords: aluminum alloy; ultrafine-grained microstructure; superplasticity; dynamic grain growth; cavitation fracture

1. Introduction

Al-Mg alloys boast a wide array of applications in aircraft industry, rocket engineering, and shipbuilding [1-11]. Aluminum alloys with 6%Mg display a good combination of strength and ductility at room temperature, as well as improved corrosion resistance. Al-6%Mg alloys are doped with scandium and zirconium to increase strength, ductility, corrosion resistance, and weldability [12-38]. Some commercial and novel Al-Mg-(Sc,Zr) alloys shows higher superplastic characteristics [36,39-52]. Industrial Al-6%Mg-(Sc,Zr) alloys enjoy an optimal combination of performance characteristics but their active commercialization is constrained by high prices for scandium and Sc-doped alloys.

Nowadays much effort is taken to find ways to replace scandium with cheaper rare earth elements (REE) and transition metals (TM) [23-24,32-34,38,43,53]. The effect of Zr [23-25,29,30,32-35,39,51,52,53,69,70], Er [53,54,56,59-61,63,66,71,76], Hf [25,53,54,57,63,70,76], Yb [53,55,62,65,66,73], and Y [54,58,64,66,67,72,74,75] is studied thoroughly, including the combined effect of several doping elements on the kinetics of precipitation and growth of particles with $L1_2$ structure in aluminum alloys. Some works are worth mentioning as they demonstrate that precipitation of $L1_2$ particles in new alloys can develop in line with the discontinuous precipitation mechanism [51,61,77-83]. The microstructure and mechanical properties of fine-grained aluminum alloys, simultaneously doped with several REEs and TMs, were studied in detail in [21-32,34,43,52,54,56-58,60,61,63,65-70,72-74,76].

Preprints (www.preprints.org) | NOT PEER-REVIEWED | Posted: 20 December 2022 doi:10.20944/preprints202212.0355.v1

Much research focuses of superplasticity of fine-grained and ultrafine-grained (UFG) Al-Mg alloys doped with REE and PM [43,82-110]. The literature review shows that UFG Al-Mg-(Sc,Zr) alloys, including industrial alloys [88,99,106,108,109], demonstrate the highest superplasticity characteristics. High superplasticity characteristics of UFG Al-Mg-(Sc,Zr) alloys system from high stability of their UFG microstructure at elevated deformation temperatures. According to [111-114], small grains intensify grain boundary sliding (GBS) rate, GBS being the main mechanism of superplastic deformation in UFG aluminum alloys. A highly stable UFG microstructure when heated and low dynamic grain growth rate in UFG Al-Mg-(Sc,Zr) alloys are explained by precipitation of $Al_3(Sc,Zr)$ nanoparticles during heating. It should be noted that large particles that form as a result of discontinuous precipitation can lead to accelerated cavitation fracture of fine-grained aluminum alloys subjected to superplastic deformation [82,83].

This research aims to study superplastic characteristics of UFG Al-6%Mg-Sc-Zr alloys with different Sc:Zr ratios.

2. Materials and Methods

The study focused on Al-6%Mg-Sc-Zr alloys with total content of Sc + Zr = 0.32 wt.%. The content of Sc and Zr in these alloys changed with an increment of 0.02 wt.%, however, total content remained constant Sc + Zr = 0.32 wt.%. The chemical composition of the alloys under study is presented in Table 1.

Table 1. Aluminum alloys: Chemical composition and casting modes.

Alloy No.	Doping elements, wt.% / at.% [1] Sc	Zr	∑	Casting modes
1	0.10 0.060	0.22 0.065	0.32 0.125	Argon purging before melting: 3 cycles Argon purging while heating: 3 cycles Induction stirring Cooling: 50–250 s, under vibration Time to melt: 6–10 min Melt temperature: 800 °C Holding time before pouring: 60 min Pouring temperature: 760 °C
2	0.12 0.072	0.20 0.059	0.32 0.131	
3	0.14 0.084	0.18 0.053	0.32 0.137	
4	0.16 0.096	0.16 0.047	0.32 0.143	
5	0.18 0.108	0.14 0.041	0.32 0.149	
6	0.20 0.120	0.12 0.035	0.32 0.156	
7	0.22 0.132	0.10 0.030	0.32 0.162	

[1] Numerator – compositions in wt.%, denominator – cmpositions in at.%.

Aluminum alloy workpieces of 20×20×160 mm were obtained by vacuum induction casting in line with the modes indicated in Table 1. An Indutherm Vacuum Tilt Casting Machine – VTC 200V (Germany) was used to produce ingots that were cast in a copper mold of 22×22×160 mm. A 150 cm^3 ceramic crucible was used. The alloys were made from aluminum grade A99. Master alloys as Al-10%Zr and Al-2%Sc were obtained by induction casting followed by rolling into a foil 0.2 mm thick.

The above workpieces were subjected to 3 cycles of Equal Channel Angular Pressing (ECAP, see [115-117]) to form a UFG microstructure. ECAP was performed at 275 ºC using a Ficep HF400L hydraulic press (Italy). Pressing was arranged using square-section tooling, with a channel intersection angle of 90°. ECAP was performed in line with B mode and a strain rate of 0.4 mm/s.

The resulting flat specimens shaped as a double blade ("dogbone-shaped") with a working part of 2×2×3 mm were subjected to mechanical tests. Tensile tests were conducted using a Tinius Olsen H25K-S machine at a strain rate of $3.3{\cdot}10^{-3}$ s^{-1} (tensile rate of

Preprints (www.preprints.org) | NOT PEER-REVIEWED | Posted: 20 December 2022 doi:10.20944/preprints202212.0355.v1

10^{-2} mm/s). Tests were run at temperatures ranging from 30 to 500 ºC. Additionally, at 400, 450, and 500 °C, the effect of strain rate ($3.3\cdot10^{-3}$, $3.3\cdot10^{-2}$, $3.3\cdot10^{-1}$ s^{-1}) on superplasticity characteristics in UFG alloys was studied. While testing, stress (σ)–strain (ε) curve was being registered and used to determine ultimate tensile strength (σ_b) and elongation to failure (δ), as well uniform strain (ε_q) corresponding to ultimate tensile strength.

Microstructure of the alloys was studied with a Leica DM IRM metallographic microscope, a Jeol JSM-6490 scanning electron microscope (SEM), and a Jeol JEM-2100F transmission electron microscope (TEM). The fractographic analysis that followed tensile tests was performed using a Jeol JSM-6490 SEM. Microstructure of the specimens after tensile tests was studied using a Leica IM DRM metallographic microscope. Microhardness (Hv) was measured using a Qness A50+ hardness tester under a 50 g load. The average accuracy of Hv measurement was ±15 MPa. Microstructure studies and microhardness measurements were carried out in the fracture area (Zone I in Fig. 1) and in the undeformed area (Zone II in Fig. 1) of the specimen.

Figure 1. General view of the UFG aluminum alloy No. 6 specimen after superplasticity tests at 450 ºC, $3.3\cdot10^{-2}$ s^{-1}. Studied areas are indicated with dash lines.

3. Results

3.1. Alloy microstrucutre

Figure 2 presents the results of examination of the cross section in the central part of the cast alloy specimens with different Sc:Zr ratios. Figure 2 shows that the specimens have a uniform macrostructure with a thin layer of columnar crystals along the edges of the ingot cross section. There are no large pores in the central part of the specimens. Scandium and zirconium content variations do not affect the ingot macrostructure, but reduced Sc content causes almost complete disappearance of large columnar crystals along the edges of the specimens (Fig. 2d).

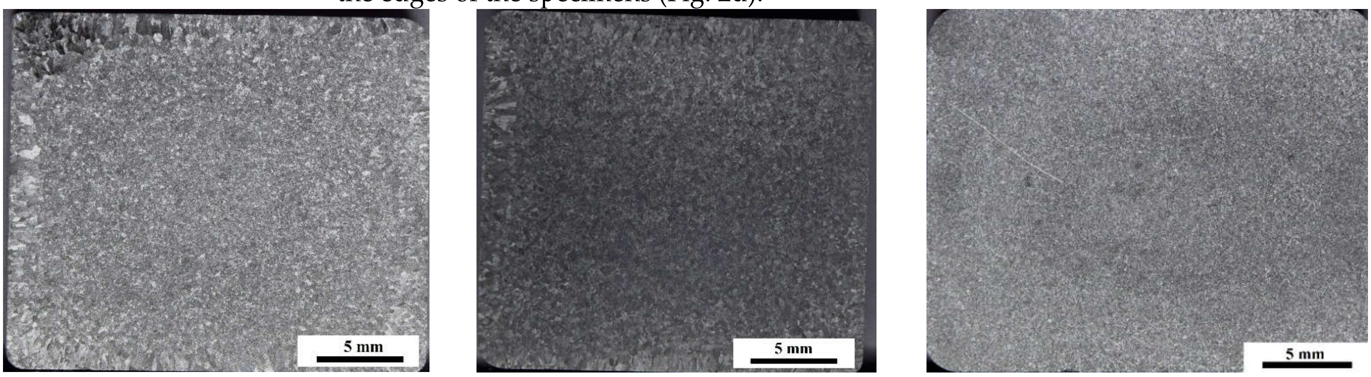

(**a**) (**b**) (**c**)

Figure 2. Macrostructure of Al-6%Mg-Sc-Zr cast alloys doped with 0.22% Sc + 0.10% Zr (**a**), 0.16% Sc + 0.16% Zr (**b**), 0.10%Sc + 0.22%Zr (**c**).

Metallography examination of the cast alloys shows that $Al_3(Sc,Zr)$ submicron primary particles form during specimen crystallization. The primary particles are evenly distributed over the cross-section surface. Rectangular primary particles with increased Zr concentration are observed in the alloys with high Zr content (Fig. 3).

Preprints (www.preprints.org) | NOT PEER-REVIEWED | Posted: 20 December 2022 doi:10.20944/preprints202212.0355.v1

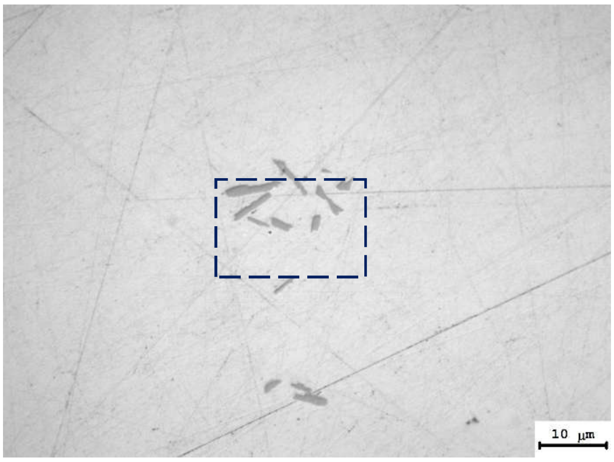

Figure 3. Primary Al_3Zr particles in Al-6%Mg-0.10%Sc-0.22%Zr cast alloy.

After ECAP, the alloys have a uniform UFG microstructure with a grain size of ~0.5–1 μm. There are no abnormally coarse grains in the alloy microstructure. Electron microscopic studies found no significant effect of Sc:Zr ratio on microstructure parameters of the UFG alloys.

3.2. Cast alloy tests

Figure 4 shows stress (σ)–strain (ε) curves for the cast alloy specimens after tensile testing at various temperatures. At low temperatures (300, 350 °C), σ(ε) curves exhibit a three-stage character: intense strain hardening followed by rapid stress relief caused by necking, reduction of cross-sectional area of a specimen. There is no stable plastic flow at low temperatures. At deformation temperatures rising to 400–450 °C, σ(ε) curves clearly show stable plastic flow. At temperatures rising from 300 to 500 °C, flow stress in the alloys goes monotonically down from 90–110 MPa to 10–12 MPa, while elongation to failure increases (Fig. 4h). It should be mentioned that as Sc content decreases and Zr concentration increases in the alloy, elongation to failure decreases (Fig. 3h) whereas flow stress changes insignificantly.

 doi:10.20944/preprints202212.0355.v1

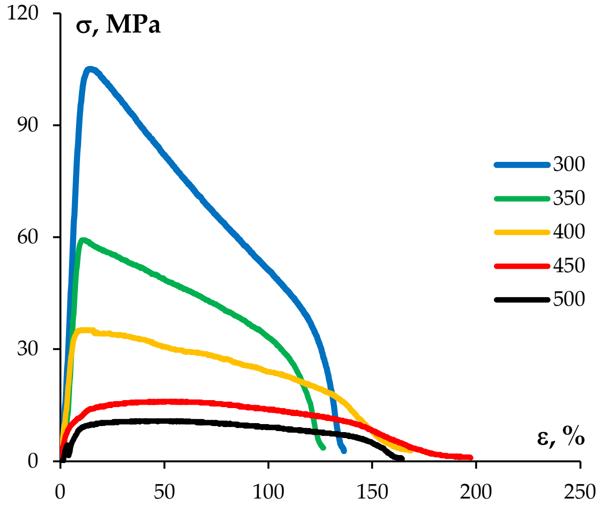

(a)

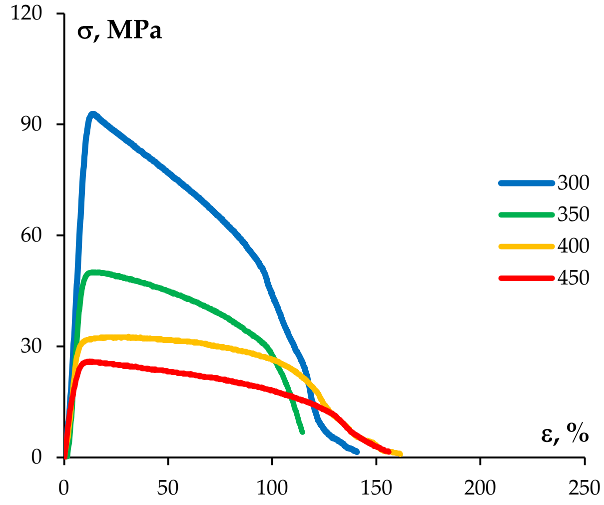

(b)

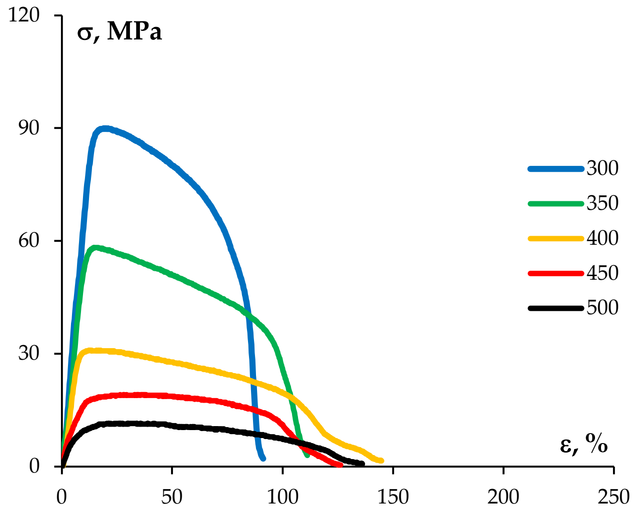

(c)

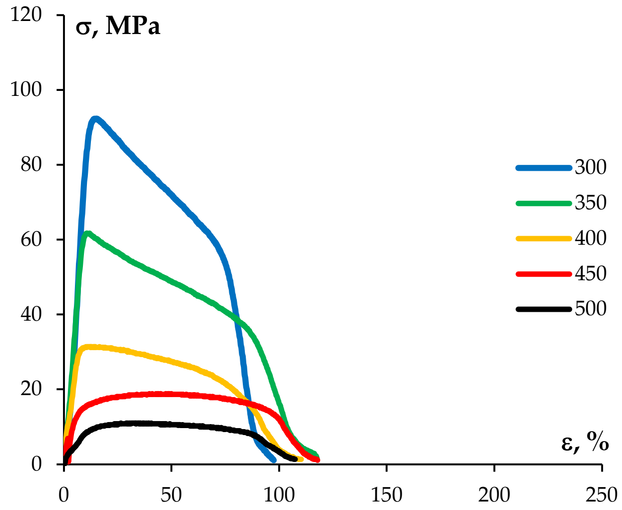

(d)

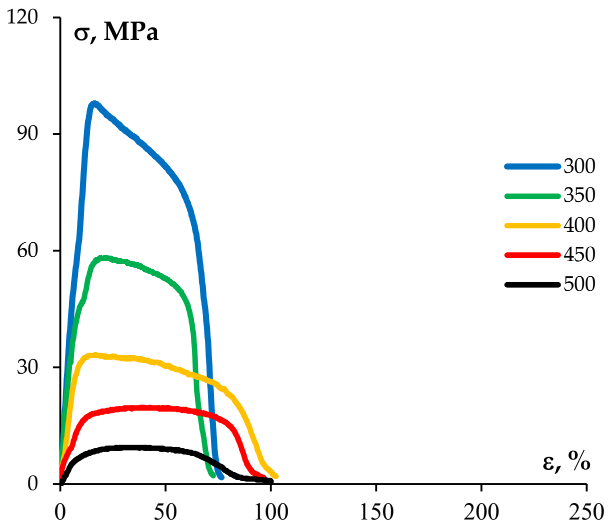

(e)

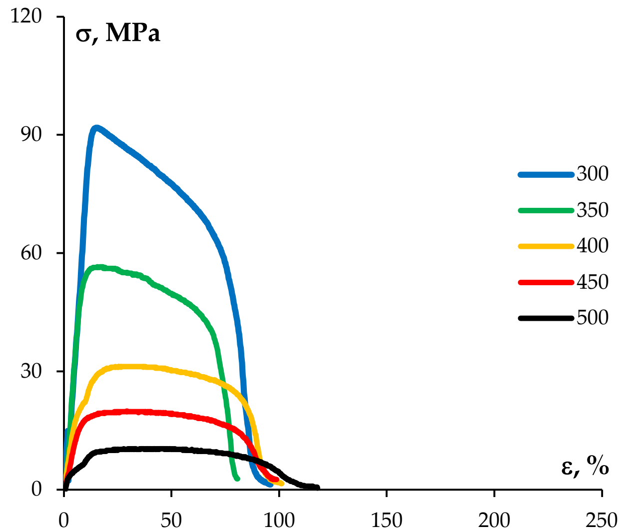

(f)

 doi:10.20944/preprints202212.0355.v1

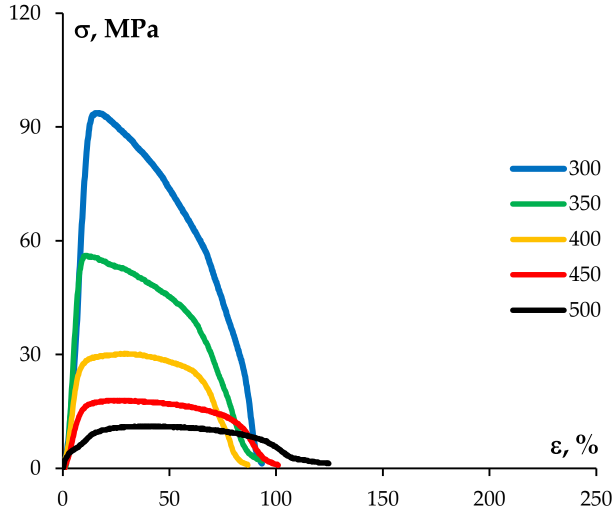

(g)

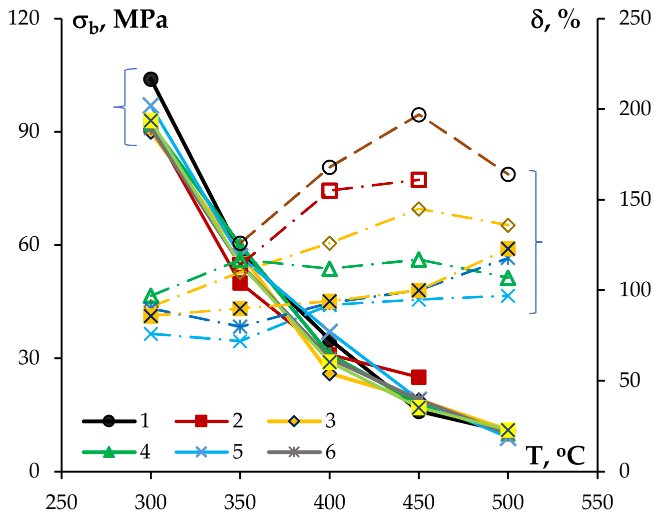

(h)

Figure 4. σ(ε) tensile curves for Al-6%Mg-Sc-Zr cast alloys Nos. 1 (**a**), 2 (**b**), 3 (**c**), 4 (**d**), 5 (**e**), 6 (**f**), and 7 (**g**) as well as dependence of flow stress (solid lines) and elongation to failure (dash lines) on deformation temperature (**h**). Strain rate of $3.3 \cdot 10^{-3}$ s^{-1}. Deformation temperatures are indicated on the charts.

The cast specimens tested at low temperatures (300, 350 °C) have oblique fractures with an angle of about 45°. Intergranular fracture is observed. At 450 and 500°C, steps (small grooves) are visible on the tips of elongated fracture fragments. Higher test temperatures hardly reduce the fracture area. No significant differences in the nature of fractures found in the cast aluminum alloy specimens of different chemical composition are observed (Fig. 5). Ductility of some alloys at 500 °C goes down because fracture starts along dendrite boundaries (Fig. 6).

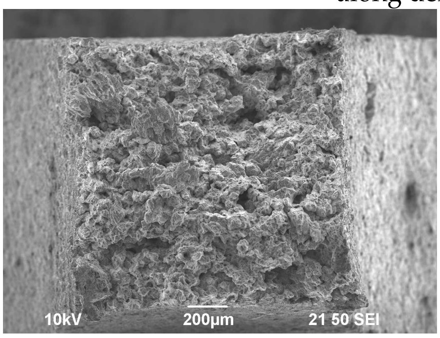

(**a**)

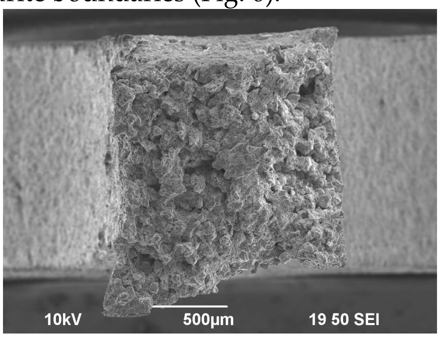

(**b**)

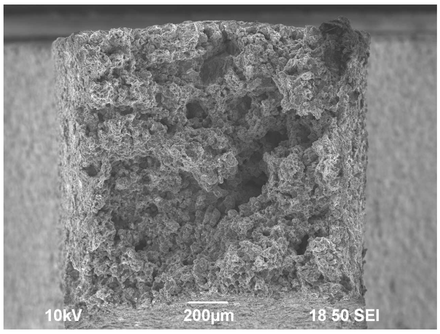

(**c**)

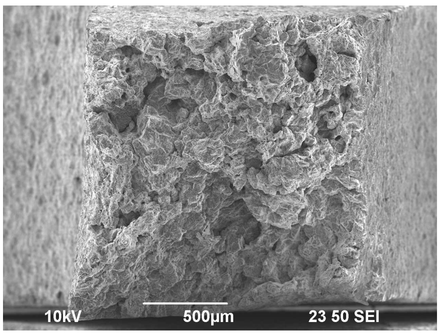

(**d**)

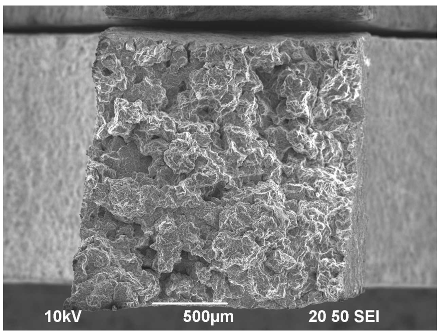

(**e**)

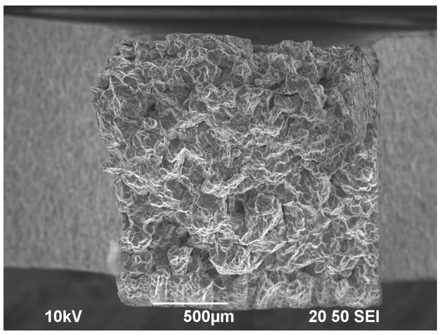

(**f**)

Figure 5. Fractographic analysis of cast alloy specimens No. 1 (**a**, **b**, **c**) and No. 7 (**d**, **e**, **f**) after testing at 300 (**a**, **d**), 400 (**b**, **e**) and 500 °C (**c**, **f**). SEM.

Preprints (www.preprints.org) | NOT PEER-REVIEWED | Posted: 20 December 2022 doi:10.20944/preprints202212.0355.v1

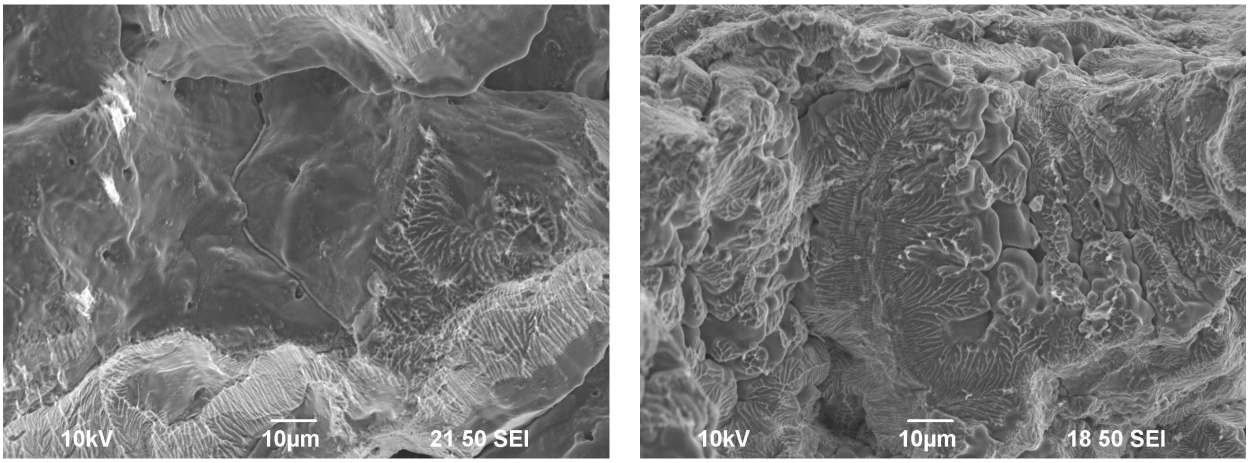

(**a**) (**b**)

Figure 6. Dendrite fragments on the surface of fractures in cast alloy specimens No. 1 (**a**) and No. 7 (**b**) after testing at 500 °C. SEM.

3.3. UFG alloy tests

Figure 7 displays σ(ε) curves for the UFG alloys tested at 300-500°C and at a strain rate of $3.3 \cdot 10^{-3}$ s^{-1}. Figure 7 shows that at 300 °C, intense strain hardening starts, which is quite typical of hot deformation in heavily deformed metals. With deformation temperature rising, flow stress decreases (Table 2), while σ(ε) curves take shape typical of superplastic deformation: a relatively short stage of homogeneous (uniform) deformation (less than 200%) is followed by softening that gives way to superplastic flow. All specimens at the stage of softening and plastic flow undergo homogeneous (uniform) deformation, without forming macroscopic necks (Fig. 1). The duration of stable plastic deformation contributes the most to the total elongation to failure in the UFG alloys (Fig. 7).

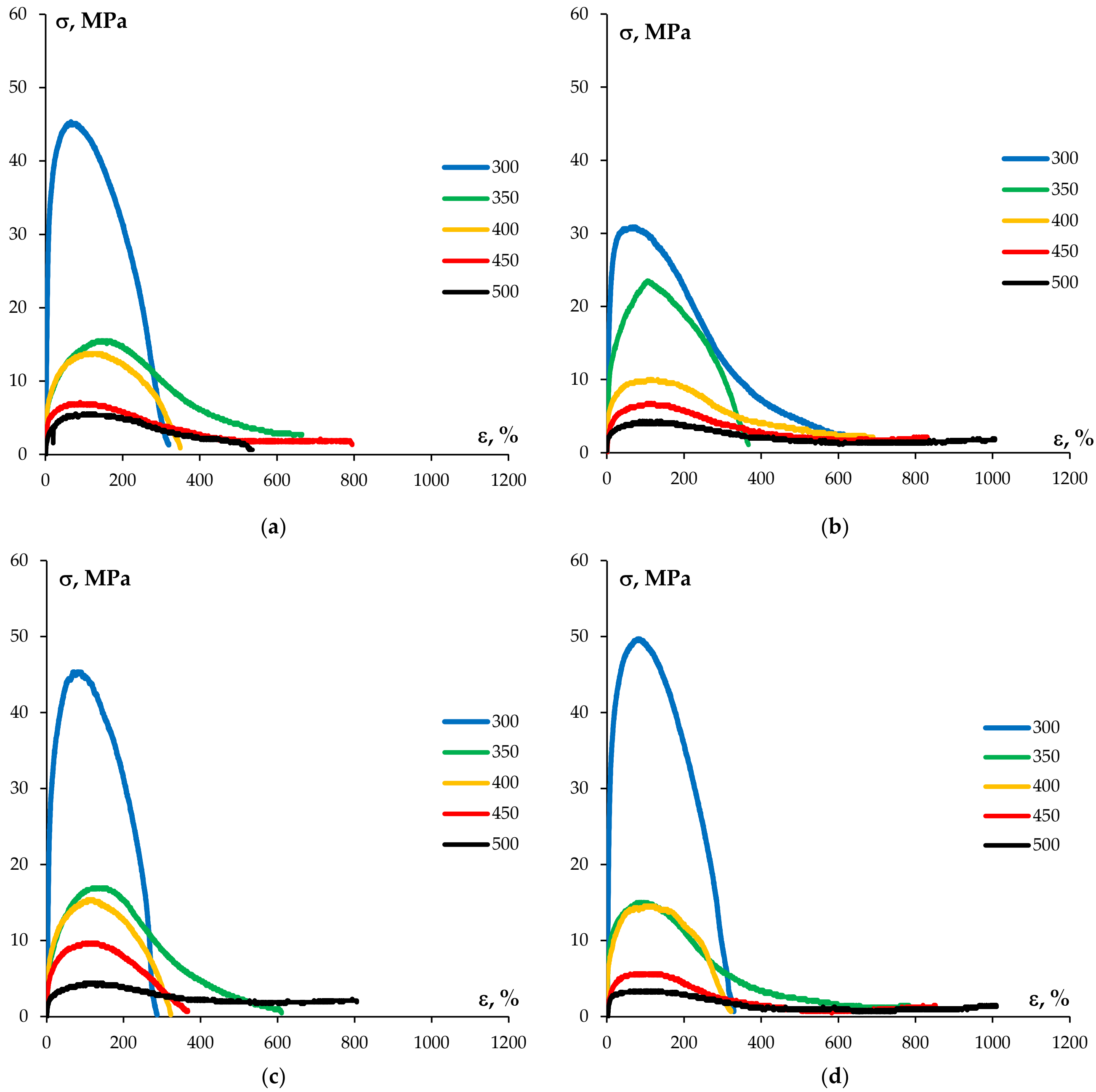
σ, MPa
ε, %
300
350
400
450
500
(a)
(b)
(c)
(d)

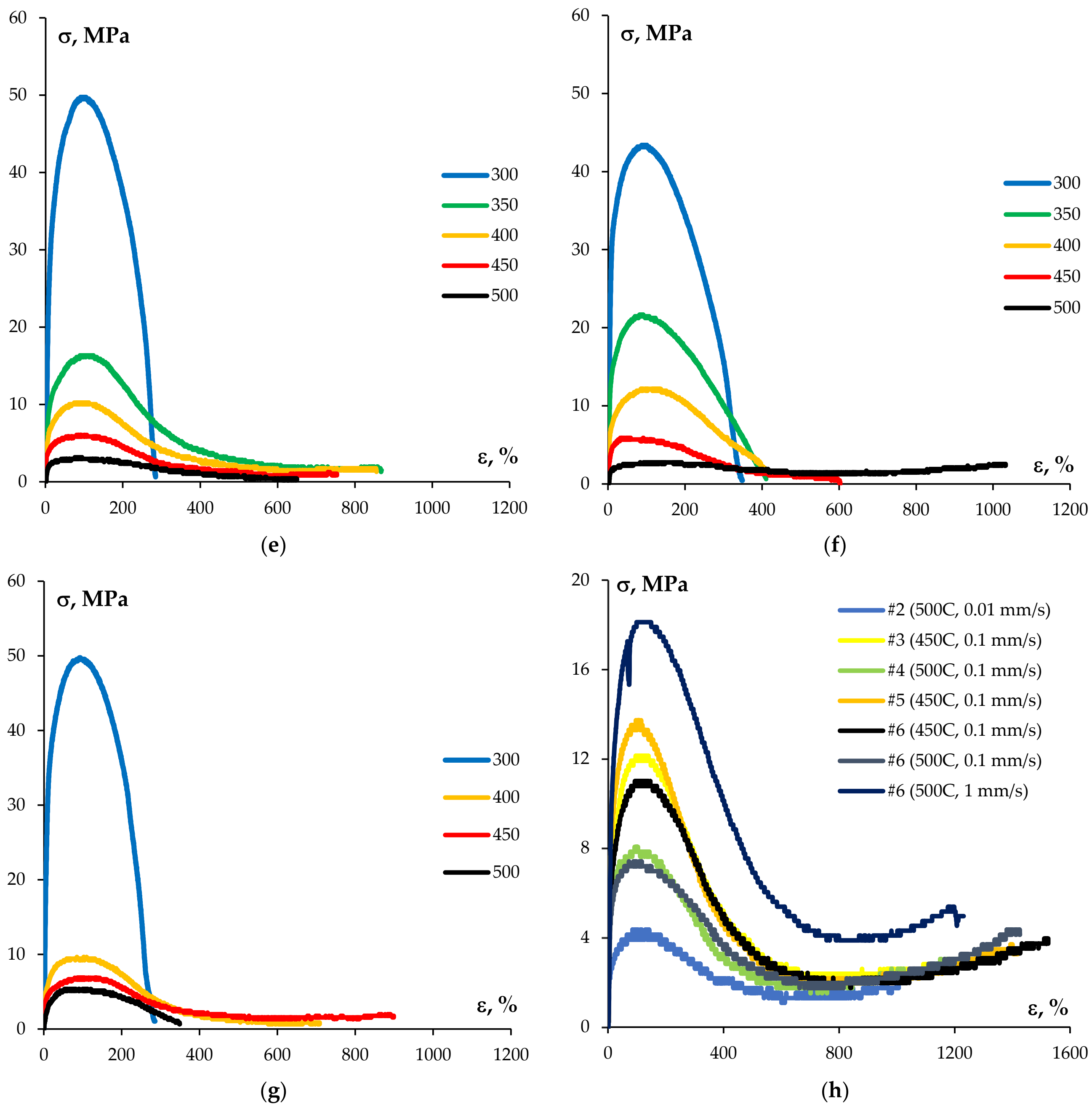

Figure 7. σ(ε) tensile curves for UFG alloys No. 1 (**a**), 2 (**b**), 3 (**c**), 4 (**d**), 5 (**e**), 6 (**f**), 7 (**g**) at a strain rate of $3.3{\cdot}10^{-3}$ s^{-1}, as well as σ(ε) curves for the UFG alloys that display elongation to failure of over 1000% (**h**) when subjected to superplastic deformation.

It is notable that in the UFG alloys whose elongation to failure exceeds 1000%, σ(ε) curves exhibit only slight stress increase at severe strains (Fig. 7h). Maximum stress under superplastic deformation is small, and at 500°C and a strain rate of $3.3{\cdot}10^{-3}$ s^{-1}, it does not exceed 7 MPa for all the UFG alloys under study (Table 2). With a strain rate rising to $3.3{\cdot}10^{-1}$ s^{-1}, differences in flow stress for the alloys become more noticeable (Table 2, Fig. 7h). Minimum flow stress and maximum elongation to failure are observed in UFG alloy No. 6. At 450°C and a strain rate of $3.3{\cdot}10^{-2}$ s^{-1} (0.1 mm/s), elongation to failure in UFG alloy No. 6 exceeds 1500%, while at 500°C, it exceeds 1400%.

Table 2. Effect of strain rate and temperature on superplasticity of the UFG alloys: flow stress σ_b [MPa] / uniform strain ε_{eq} [%] / elongation to failure δ [%].

T, °C	**300**	**350**		**400**			**450**			**500**	
$\dot{\varepsilon}$, s^{-1}	$3.3{\cdot}10^{-3}$	$3.3{\cdot}10^{-3}$	$3.3{\cdot}10^{-3}$	$3.3{\cdot}10^{-2}$	$3.3{\cdot}10^{-1}$	$3.3{\cdot}10^{-3}$	$3.3{\cdot}10^{-2}$	$3.3{\cdot}10^{-1}$	$3.3{\cdot}10^{-3}$	$3.3{\cdot}10^{-2}$	$3.3{\cdot}10^{-1}$
Alloy No.											
	45 [1]	15	14	32	62	7	15	44	5	9	28
1	70 [2]	175	145	105	70	130	125	75	175	135	100
	320 [3]	680	350	350	330	800	600	400	520	700	390
	31 [1]	23	10	35	58	7	20	38	4	14	26
2	75 [2]	120	140	115	100	135	120	100	185	110	100
	660 [3]	370	660	405	440	820	350	480	1000	320	550
	48 [1]	17	15	37	68	9	12	52	4	14	23
3	90 [2]	170	125	105	90	135	145	75	185	110	120
	300 [3]	600	320	320	380	370	1100	205	800	340	640
	50 [1]	15	14	22	60	6	23	48	4	8	32
4	95 [2]	115	175	140	100	170	110	100	190	165	95
	330 [3]	780	320	900	430	850	290	210	1010	1220	185
	50 [1]	16	10	35	78	6	14	33	3	14	33
5	110 [2]	125	115	115	65	140	135	100	200	130	95
	285 [3]	860	850	250	220	750	1420	810	650	300	180
	44 [1]	22	12	28	74	6	11	31	3	7	18
6	110 [2]	105	135	130	85	170	170	140	270	140	170
	350 [3]	410	410	380	275	600	1520	910	1030	1420	1230
	50 [1]	16	9	19	57	7	22	48	5	14	23
7	120 [2]	120	140	120	95	170	130	120	170	160	145
	285 [3]	690	700	780	410	900	330	160	350	400	860

[1] flow stress σ_b [MPa]. [2] uniform strain ε_{eq} [%]. [3] elongation to failure δ [%].

It is worth mentioning that superplastic deformation of the UFG aluminum alloys is accompanied by intense pore formation (cavitation) (Fig. 8). At a given ratio of scandium and zirconium (Sc:Zr = const), an increase in the strain leads to an increase in the volume fraction and size of pores. Higher Zr content and lower Sc concentration reduce the tendency of the UFG alloys to pore formation (Fig. 8). Pores are evenly distributed along the deformed part of the specimen, from the fracture area to the undeformed area, in accordance with strain distribution in the specimen. If microscopic localized plastic flow occurs, local areas of the smallest cross section display an increased amount and size of pores (Fig. 9). Metallographic studies show that pores are found mainly along grain boundaries of the UFG alloys (Fig. 10).

 doi:10.20944/preprints202212.0355.v1

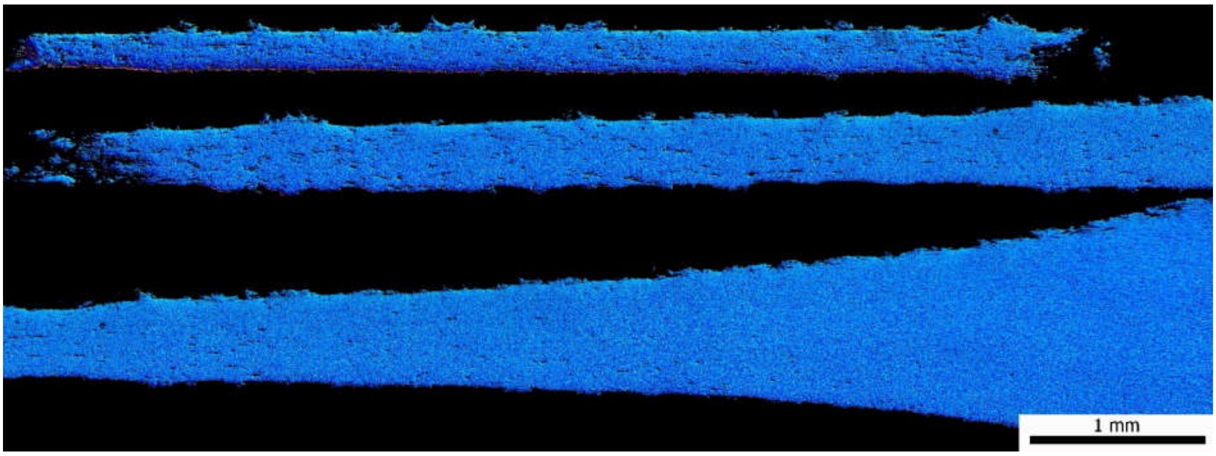

(**a**)

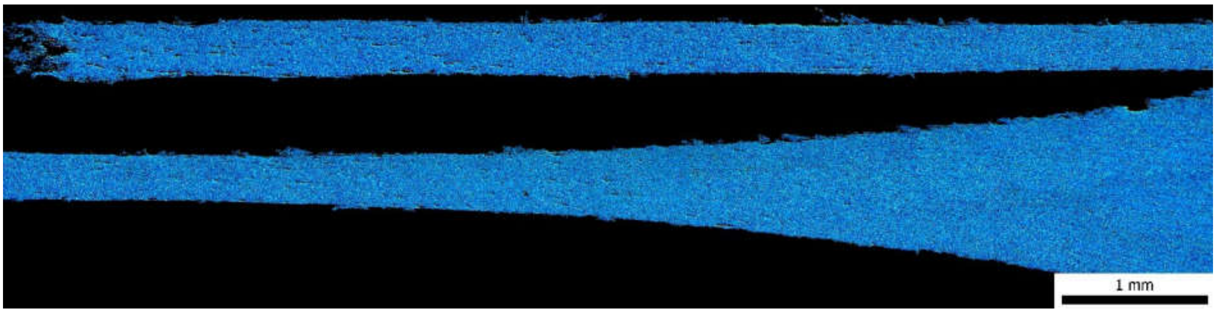

(**b**)

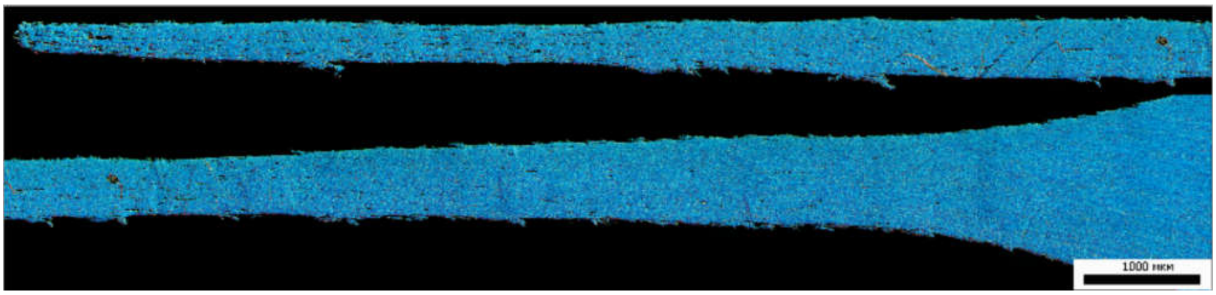

(**c**)

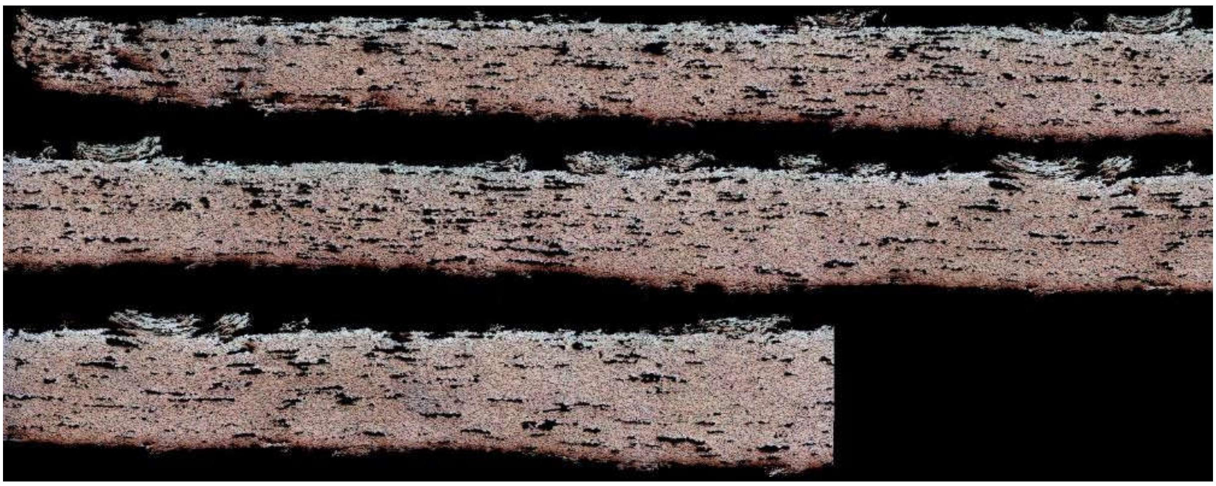

(**d**)

Figure 8. General view of the aluminum alloy specimens after superplasticity tests: (a) alloy No.2 (450 ^{o}C, 3.3·10^{-2} s^{-1}), (b) alloy No.3 (450 ^{o}C, 3.3·10^{-2} s^{-1}), (c) alloy No.5 (450 ^{o}C, 3.3·10^{-2} s^{-1}), (d) No.7 (450 ^{o}C, 3.3·10^{-3} s^{-1}).

Preprints (www.preprints.org) | NOT PEER-REVIEWED | Posted: 20 December 2022 doi:10.20944/preprints202212.0355.v1

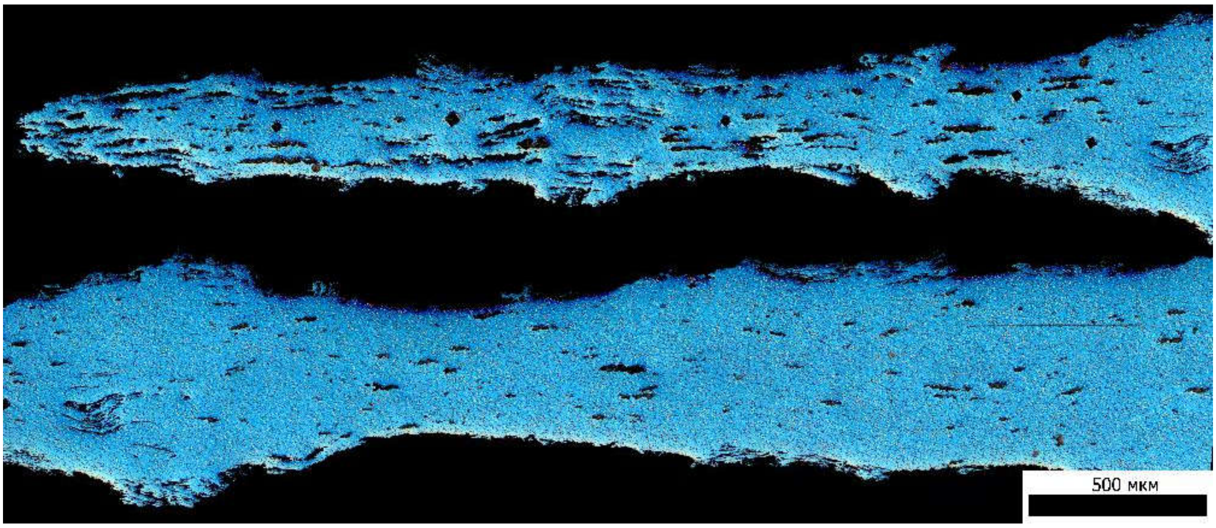

(**a**)

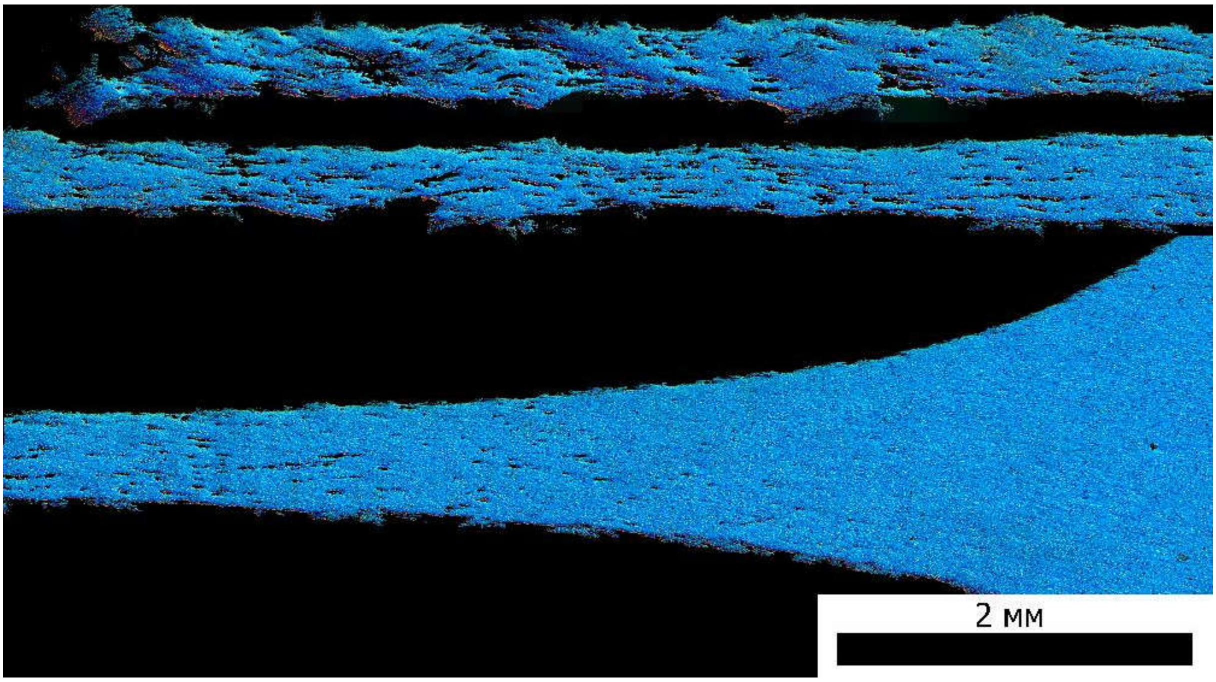

(**b**)

Figure 9. General view of the UFG alloy specimens after superplasticity tests: (a) alloy No.5 (500 ^{o}C, $3.3{\cdot}10^{-3}$ s^{-1}); (b) alloy No.6 (500 ^{o}C, $3.3{\cdot}10^{-3}$ s^{-1}).

Figure 10 and Table 2 present the results of studies of grain growth under superplastic deformation of the UFG alloys with different Sc:Zr ratios. Figure 11 and Table 2 show that Sc:Zr ratio has a significant effect on microstructure evolution in the aluminum alloys under superplastic deformation. The alloys with high Zr content at elevated temperatures are characterized by abnormal grain growth: the average grain size can reach 100 μm. Pores often occur along the boundaries of abnormally coarse grains (Fig. 11b).

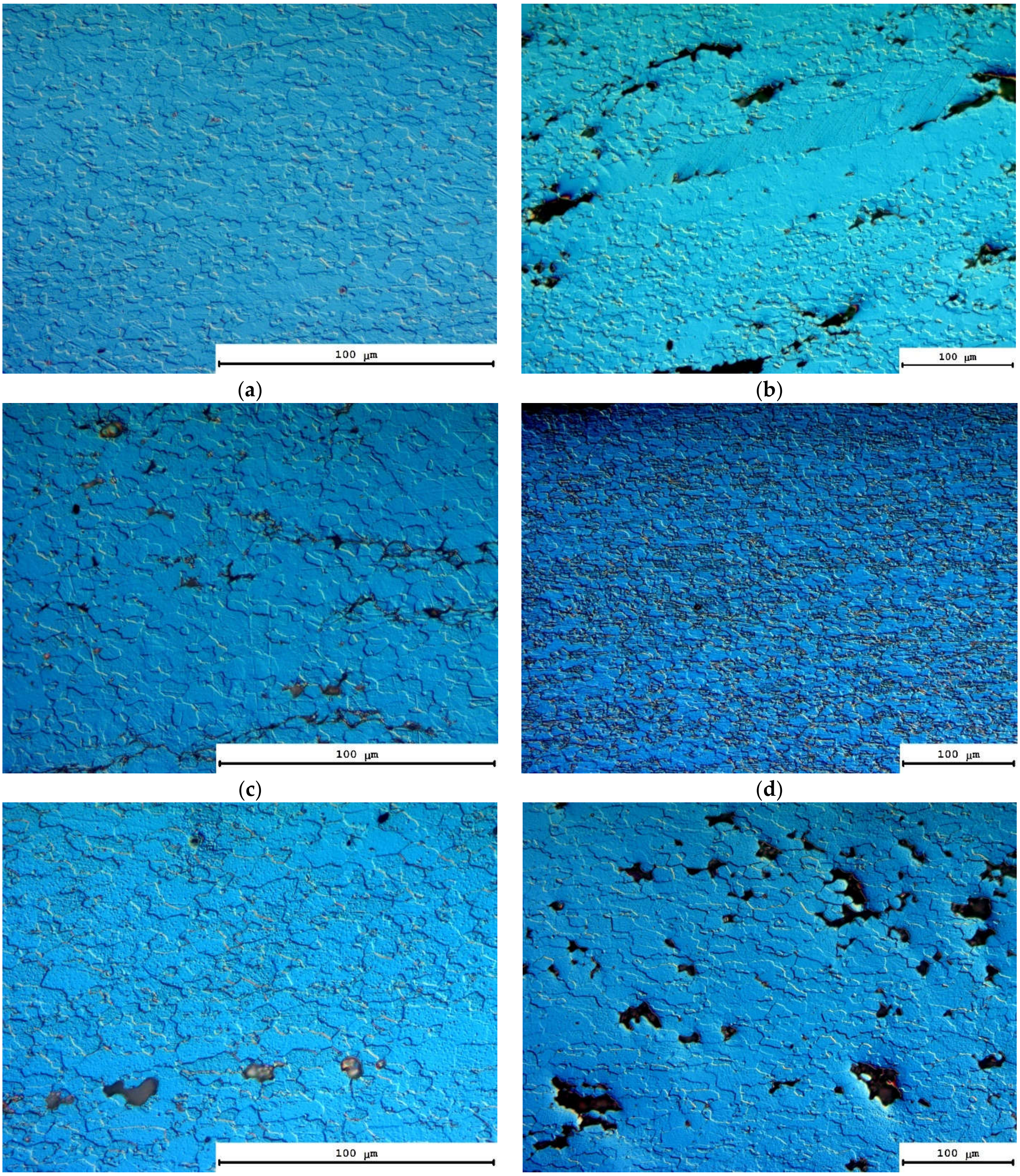

Figure 10. Microstructure of the deformed part of alloy specimens No. 1 (**a**, **b**), No. 2 (**c**, **d**) and No. 7 (**e**, **f**) after testing at 450 °C (a, c, e) and 500 °C (b, d, f). Strain rate of $3.3 \cdot 10^{-3}$ s^{-1}.

The analysis of results presented in Table 2 shows that a decrease in Sc content in the UFG alloys causes a slight increase in the average grain size in the strained zone, close to the fracture area. There is no definite dependence of the average grain size in the undeformed part of the specimen on Sc:Zr ratio. This is obviously due to differences in testing times, which depend on the degree of elongation to failure in the specimens.

It is crucial that ECAP is accompanied by the formation of macroscopic shear bands. At small strain (few ECAP cycles), this leads to inhomogeneous strain distribution in the specimen and consequently to inhomogeneous recrystallization processes. The characteristic width of macroscopic shear bands can reach 0.5 mm. By way of example, Figure 11 shows the results of metallography examination in two adjacent areas of the undeformed part of the specimens. Figure 11 shows that the microstructure in two neighboring areas of Zone I (see Fig. 1) can vary significantly.

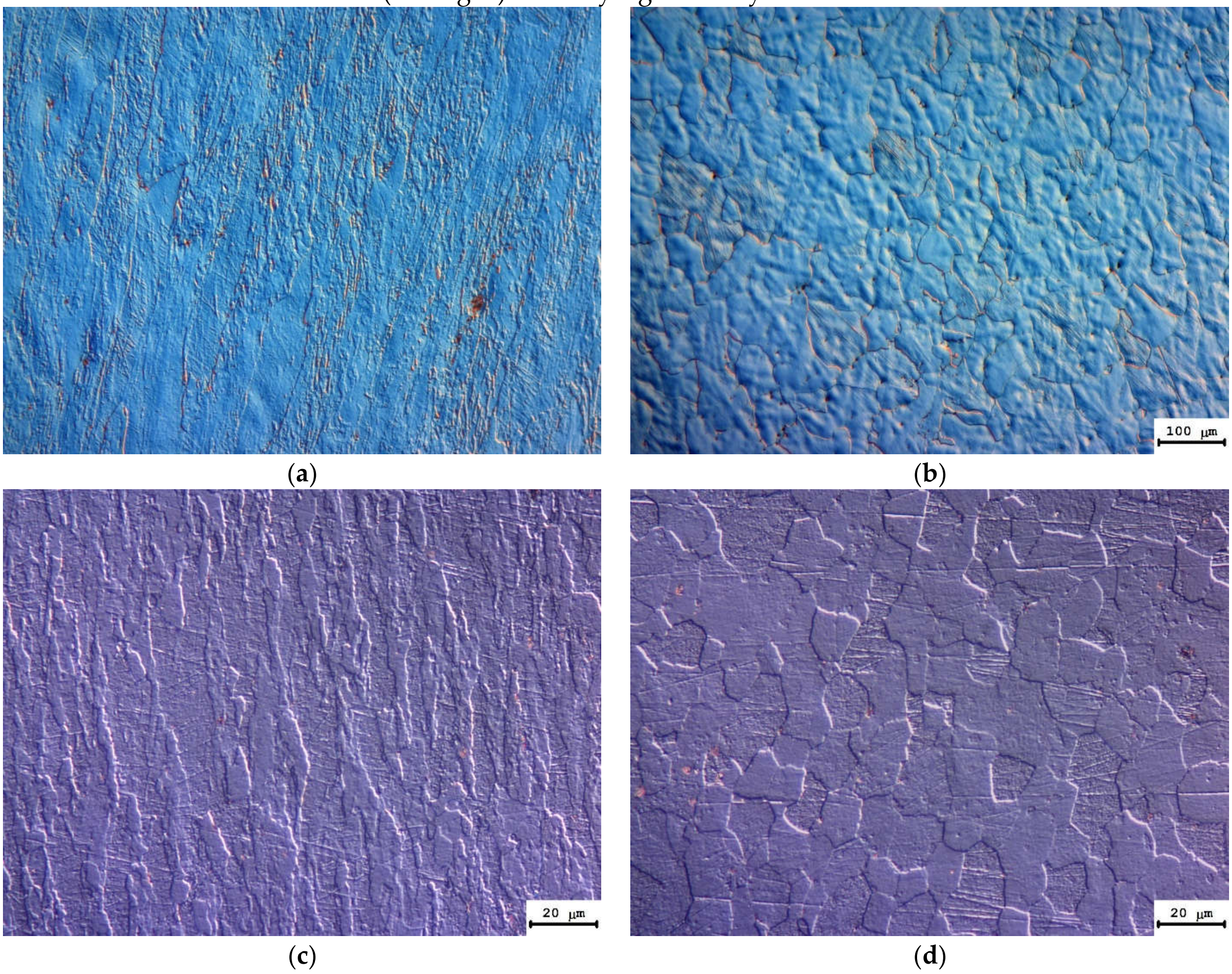

Figure 11. Microstructure of the undeformed part of alloy specimens No. 1 (**a**, **b**) and No. 7 (**c**, **d**) after superplasticity testing: (**a**, **b**) – 450 °C, $3.3 \cdot 10^{-2}$ s^{-1}, (**c d**) – 400 °C, $3.3 \cdot 10^{-2}$ s^{-1}.

It should be noted that despite significant microstructure inhomogeneity in Zone I, the average grain size in the fracture area turns out to be several times smaller than the average grain size in the undeformed area of the specimen (Table 3). The results obtained prove that there is no strain-induced grain growth in the studied materials. We reckon that dynamic recrystallization is the most probable microstructure evolution mechanism in the UFG aluminum alloys under superplasticity, which corresponds to the results presented in [96,118,119].

Table 3. Results of studying grain size in the UFG alloy specimens after superplasticity testing. Numerator: average grain size in the undeformed area (Zone I in Fig. 1), denominator: average grain size in the deformed area (Zone II in Fig. 1).

Alloy No.	T, °C	300	350	400			450			500		
	$\dot{\varepsilon}$, s^{-1}	$3.3{\cdot}10^{-3}$	$3.3{\cdot}10^{-3}$	$3.3{\cdot}10^{-3}$	$3.3{\cdot}10^{-2}$	$3.3{\cdot}10^{-1}$	$3.3{\cdot}10^{-3}$	$3.3{\cdot}10^{-2}$	$3.3{\cdot}10^{-1}$	$3.3{\cdot}10^{-3}$	$3.3{\cdot}10^{-2}$	$3.3{\cdot}10^{-1}$
	1	15-20	15-20	15-20	15-20	15	15-20	15-20	15	15-20	15-20	15
		0.5-1	2.1	2.7	3.0	2.0	3.7	3.0	2.6	7.0	3.8	2.4
	2	15-20	15-20	15-20	15	15	15-20	15-20	15	20-25	20	15-20
		1.9	1.9	2.8	2.3	1.4	3.4	4.3	1.8	6.3	5.1	2.5
	3	30	30-35	30-40	30-40	30-35	50	35-45	25-35	45-50	40-50	35-45
		1.6	1.9	2.3	2.2	1.3	2.5	2.5	2.4-2.5	5.5	2.5	2.3
	4	20-25	25	25-35	25-30	25	45-55	40-50	40-45	50	40-50	30-50
		1.2	2.3	3.1	2.6	1.5	3.8	2.5	2.3	6.3	3.3	2.1
	5	15-20	15-20	-	-	-	10	5-10	5-10	10	5-10	5-10
		1.4	2.2	2.9	2.2	2.2	3.6	2.8	1.9	4.5	2.7	2.2
	6	10-20	15-20	20-25	20	20	20-30	20-25	20-25	30	25-30	25
		1.5	1.6	2.3	1.6	1.4	3.6	2.7	1.8	4.4	3.9	2.8
	7	50	50	50-70	50	50	50-100	50-70	50	100-150	100-120	100
		0.5-1	1.7	2.2	1.3	1.2	2.6	2.3	0.5-1	3.7	2.7	2.3

[1] average grain size in the undeformed area (Zone II in Fig. 1); [2] average grain size in the deformed area (Zone I in Fig. 1).

Microhardness studies in the UFG alloy specimens after superplasticity testing yield quite unexpected results. Figure 12 reveals the dependences of microhardness Hv on deformation temperature for deformed (Fig. 12a) and undeformed (Fig. 12b) areas in the UFG alloy specimens. Hv(T) dependence for the undeformed part of the specimens has a conventional two-stage character, microhardness values reach maximum after deformation at 350°C. Microhardness values reach maximum after deformation in alloys No. 5-7 at 350 °C (Fig. 12a). With temperatures rising, microhardness values for the undeformed part of the specimens decrease (Fig. 1a). With deformation temperatures rising, microhardness values for the deformed part of the specimens decrease monotonically (Fig. 12b). It is noteworthy that hardness values in the fracture area after deformation at 450–500 °C turn out to be less than those for the undeformed part of the specimens.

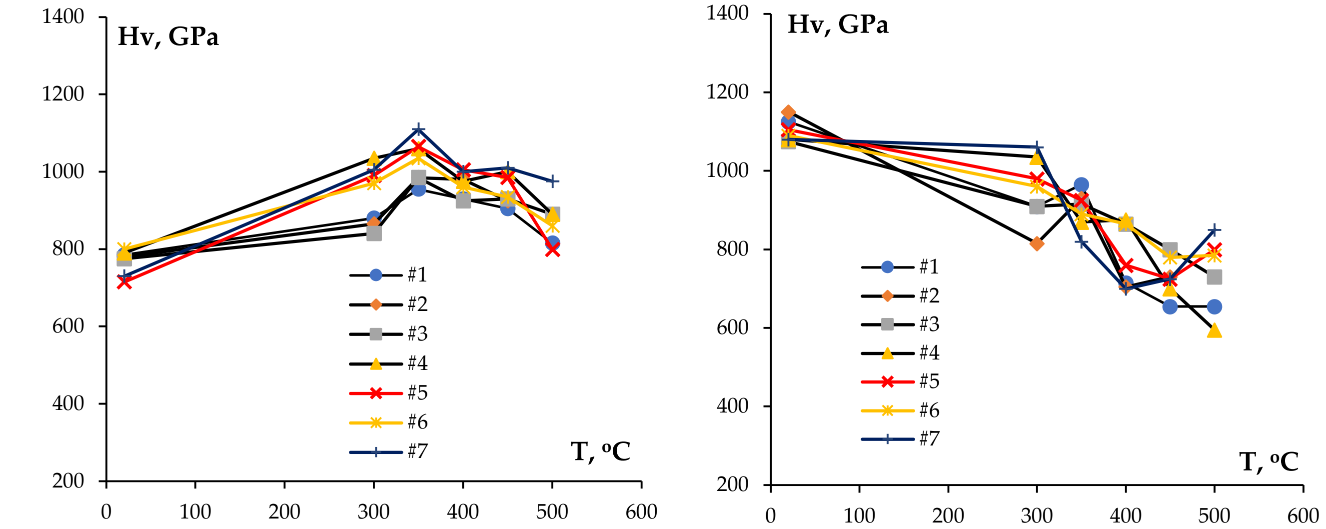

(**a**) (**b**)

Figure 12. Dependences of microhardness on testing temperature in the UFG aluminum alloys. Strain rate of $3.3{\cdot}10^{-3}$ s^{-1}. Figure 12**a**: results of microhardness studies of the undeformed part (Zone I), Figure 12**b**: results of microhardness studies of the deformed part (Zone II).

Preprints (www.preprints.org) | NOT PEER-REVIEWED | Posted: 20 December 2022 doi:10.20944/preprints202212.0355.v1

4. Discussion

Below is the preliminary analysis of possible superplastic deformation mechanisms in UFG Al-6%Mg-Sc-Zr alloys. First, we need to determine strain rate sensitivity coefficient of flow stress (m) in the following superplasticity equation for the UFG alloys:

$$\dot{\varepsilon} = A(\sigma^*/G)^{1/m}(b/d)^p(D_{eff}/b^2)(G\Omega/kT), \quad (1)$$

where m – strain rate sensitivity coefficient of flow stress that depends on strain rate $\dot{\varepsilon}$, p – numerical parameter equal to 2 or 3 [111,113]; b – Burgers vector, G – shear modulus, k – Boltzmann constant, σ^* – flow stress, D_{eff} – effective diffusion coefficient under superplasticity. It is usually assumed that $\sigma^* = \sigma_b$, $D_{eff} = D_0\exp(Q_{eff}/kT)$, where Q_{eff} – apparent activation energy of superplastic flow.

The rheological superplasticity equation can also be presented in such a way that contributions of intergranular ($\dot{\varepsilon}_b$) and intragranular deformation ($\dot{\varepsilon}_v$) are separated [111,113]:

$$\dot{\varepsilon} = \dot{\varepsilon}_b + \dot{\varepsilon}_v. \quad (2)$$

To calculate intragranular strain rate $\dot{\varepsilon}_v$, the usual power-law creep strain rate equation is used [111]. To describe grain boundary slip (GBS) rate $\dot{\varepsilon}_b$, the following equation is usually applied:

$$\dot{\varepsilon}_b = A_b(\sigma/G)^2(b/d)^2(G\Omega/kT)(\delta D_b/b^3), \quad (3)$$

where A_b – numerical coefficient equal to ~100 [111,113]. Under optimal superplasticity conditions, when GBS contributes the most to the deformation of a fine-grained material, m is usually equal to 0.5 [111].

Strain rate sensitivity coefficient $m = \ln(\sigma_b)/\ln(\dot{\varepsilon})$ can be determined by the slope of flow stress–strain rate dependence in logarithmic coordinates. The analysis of $\ln(\sigma_b) - \ln(\dot{\varepsilon})$ dependences presented in Figure 13 shows that m ranges from 0.32 to 0.42. In UFG alloy No. 6 with the highest elongation to failure observed, at 450 and 500 °C, m is 0.36 ± 0.03 and 0.39 ± 0.02, respectively. Such m value is not very high, which means that GBS and intragranular deformation make comparable contributions to superplastic flow in the UFG aluminum alloys under study. We reckon that one of the most probable reasons for this is dynamic recrystallization accompanied by grain growth (see [118,119]).

Preprints (www.preprints.org) | NOT PEER-REVIEWED | Posted: 20 December 2022 doi:10.20944/preprints202212.0355.v1

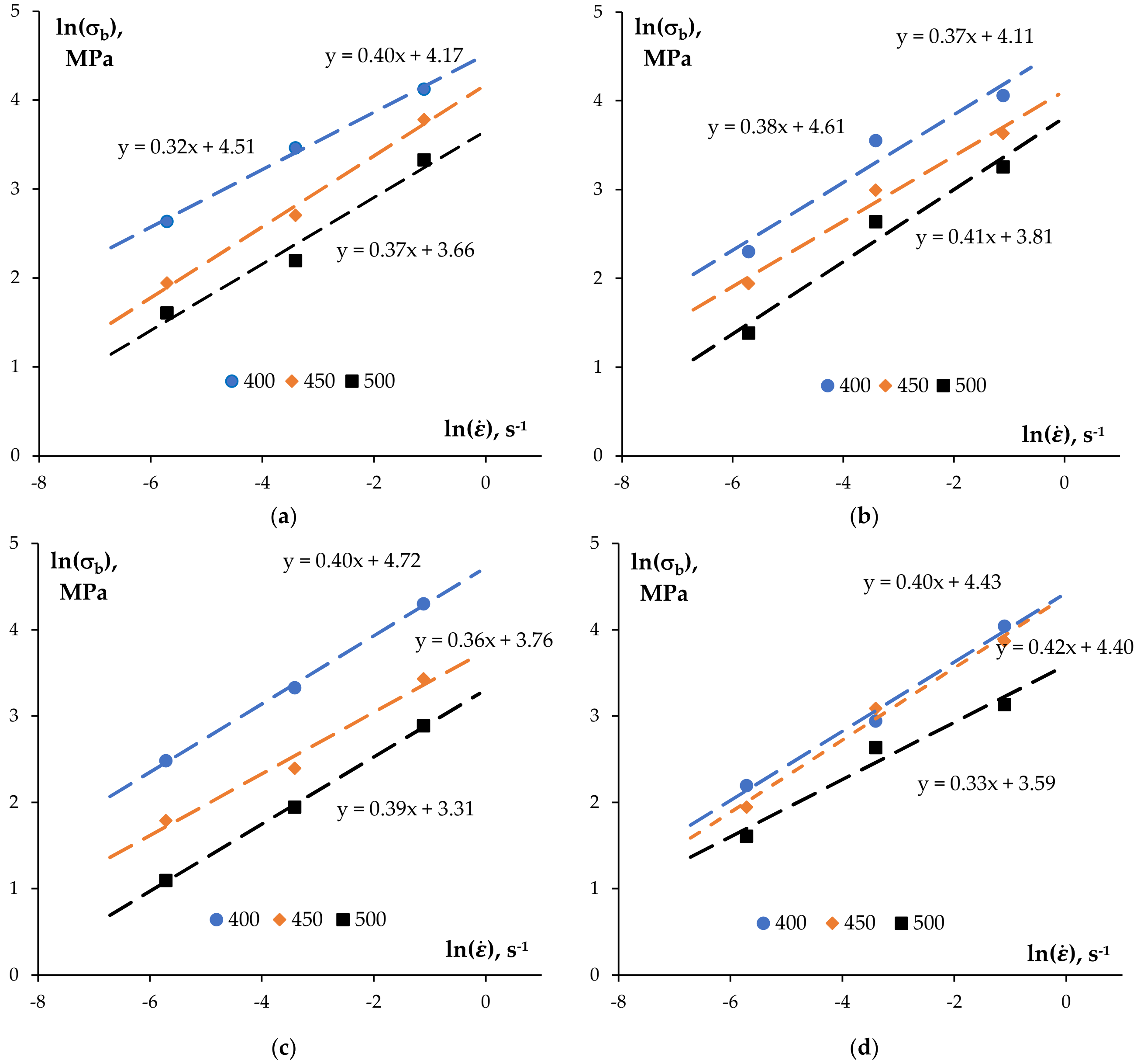

Figure 13. Flow stress–strain rate dependence in logarithmic coordinates for UFG alloys Nos. 1 (**a**), 2 (**b**), 6 (**c**), 7 (**d**).

Intense pore formation under superplasticity in UFG Al-6%Mg-Sc-Zr aluminum alloys is triggered by Al_3(Sc,Zr) secondary particles. As shown in [82,83,120,121], superplastic deformation of fine-grained alloys results in accumulated defects of secondary particles, which impede lattice dislocations and GBS. Defects of dislocation-disclination type in secondary particles are expected to trigger micropores, the size of which grows along with deformation degree and strain rate (see [120,121]). In line with the model described in [120,121], pore formation in the area of plastic deformation localization stems from increased local strain in the necking area.

The analysis of specimen surfaces after superplasticity testing shows that a decrease in Zr content and an increase in Sc concentration reduce the tendency of the UFG alloys to pore formation. We reckon that large Al_3(Sc,Zr) particles formed by discontinuous precipitation are one of the most probable reasons for this effect. As shown in [82,83], discontinuous precipitation accompanied by formation of large acicular Al_3Sc particles can be observed during annealing of the UFG alloys with high Sc content. Such particles can reach 50-200 nm in size. With Sc concentration growing, the number of large Al_3(Sc,Zr), particles formed by discontinuous precipitation increases. This leads to intensified pore formation under superplastic deformation conditions. The effect of pore formation under superplastic deformation in UFG Al-0.5%Mg-Sc alloys with large Al_3Sc particles was described in [82,83].

Another factor conducive to the formation of large particles can be differences in spatial distribution of Sc and Zr atoms in the aluminum alloy. It is known that during ingot crystallization, spatial distribution of doping elements can be described using distribution coefficient $K = C_S/C_L$, where C_S and C_L are concentrations of the doping element in the crystal lattice and in the molten metal [122]. If $K < 1$, doping elements are concentrated in the molten metal and after crystallization, they shift mostly towards grain/dendrite boundaries. If $K > 1$, doping elements are found mostly in the crystal lattice. K for Sc atoms in aluminum is K_{Sc} = 0.9-1.0, while for Zr in aluminum, K_{Zr} = 2.5 [122]. In accordance with [115], nonequilibrium grain boundaries in UFG materials can be described as melt islands (L-phase) surrounded by a crystal lattice (S-phase). This being the case, the concentration of doping elements along grain boundaries (C_b) can be linked to the concentration of doping elements in the crystal lattice (C_V) using distribution coefficient $K_C = \alpha C_v/C_b$, where α is grain boundary free (excess) volume proportional to the volume fraction of L-phase islands [115]. Thus, it can be assumed that during aluminum alloy ingot crystallization, Zr atoms may concentrate mostly in the aluminum crystal lattice, while Sc atoms may be evenly concentrate in the crystal lattice and grain / dendrite boundaries. As a result, during heating, Al_3Zr secondary particles will mostly precipitate in the crystal lattice and Al_3Sc particles will precipitate along grain boundaries (particle Al_3Sc) and in the crystal lattice (particle $Al_3(Sc,Zr)$).

In conclusion, let us analyze the effect of Sc:Zr ratio on superplastic characteristics of the UFG aluminum alloys. Table 2 shows that alloy No. 6 Al-6wt.%Mg-0.20wt.%Sc-0.12wt.%Zr (Al – 6.67 at.% Mg – 0.12 at.% Sc – 0.036 at.% Zr) with Sc:Zr ratio = 3.3 (at.%) has the highest superplasticity characteristics. Alloy No. 5 Al-6wt.%Mg-0.18wt.%Sc-0.14wt.%Zr (Al – 6.67 at.%Mg – 0.11 at.%Sc – 0.04 at.%Zr) with Sc:Zr ratio = 2.8 (at.%) has good superplasticity properties. Thus, optimal Sc:Zr ratio for Al-6%Mg alloy varies from 2.8 to 3.3. As a first approximation, it can be assumed that the average optimal Sc:Zr ratio is ~ 3 (at.%), which corresponds to $Al_3(Sc_xZr_{1-x})$ composition with $x = 0.75$.

The composition of particles in Al-Sc-Zr alloys was studied in sufficient detail in many works (see, for example, [123-135]). As shown in [136], precipitation of $Al_3(Sc_{0.5}Zr_{0.5})$ particles is more energetically favorable than that of Al_3Sc and Al_3Zr particles. $x = 0.5$ ratio corresponds to the solubility limit of Group 4 transition metal atoms in Al_3Sc particles with $L1_2$ structure [123]. As outlined in [137], there are three variants of $Al_3(Sc,Zr)$ particles precipitation: $Al_3(Sc_{0.75}Zr_{0.25})$, $Al_3(Sc_{0.5}Zr_{0.5})$, $Al_3(Sc_{0.25}Zr_{0.75})$. Production of $Al_3(Sc_{0.74}Zr_{0.26})$ intermetallic compound and its properties were described in [138]. As shown in [139-141], $Al_3(Sc,Zr)$ particles have the following structure: Al_3Sc core – Al_3Zr shell.

Let us assume that due to differences in distribution coefficients of Sc and Zr atoms in aluminum, three types of particles in the alloys under study can precipitate: Al_3Sc, Al_3Zr, $Al_3(Sc_xZr_{1-x})$. Al_3Sc particles and $Al_3(Sc_xZr_{1-x})$ variable composition particles precipitate in alloys with high Sc concentration. With Zr content growing in the alloy, Sc concentration (x) in $Al_3(Sc_xZr_{1-x})$ particles decreases and Al_3Zr particles precipitate. It is noteworthy that Zr atomic mass (91.224 a.m.u.) is almost two times bigger than Sc atomic mass (44.96 a.m.u.), therefore when 0.02 wt.% Sc is substituted with 0.02 wt.% Zr, $Al_3(Sc,Zr)$ particles rise in number. Thus, from a formal perspective, partial replacement of Sc with Zr of an equivalent mass can decrease the volume fraction of precipitating $Al_3(Sc,Zr)$ particles. High volume fraction (in at.%) of secondary $Al_3(Sc,Zr)$ particles in UFG alloys No. 5-7 (Table 1) is one of the important factors for ensuring high superplasticity characteristics in alloys with a higher scandium content.

However, the diffusion coefficient of zirconium in aluminum [142] is much less than that of scandium in aluminum [143-146]. As a result, Al_3Zr particles precipitate at higher temperatures and/or longer annealing times compared to Al_3Sc particles. Thus, hardening of Al-Zr alloys is weaker than that of Al-Sc alloys under the same annealing conditions. Precipitation of primary Al_3Zr particles is another factor conducive to a decrease in the volume fraction of Al_3Zr and $Al_3(Sc_xZr_{1-x})$ particles in alloys with high Zr content (Fig. 3). Increased content of Al_3Sc and $Al_3(Sc_xZr_{1-x})$ particles in alloys Nos. 6-7 is the most likely reason why cavitation erosion accelerates (Fig. 9) and why a finer-grained microstructure in the deformation region forms (Table 3).

Thus, Sc:Zr ratio affects superplastic characteristics of UFG Al-6%Mg-Sc-Zr alloys through a change in the composition and amount of precipitating secondary Al_3Sc, Al_3Zr, $Al_3(Sc,Zr)$ particles.

5. Conclusions

1. Deformation behavior of cast and UFG Al-6%Mg-Sc-Zr alloys with different Sc:Zr ratio (Sc + Zr = 0.32 wt.%) was researched. It was shown that peak values of elongation to failure for the UFG alloys (> 1500%) are several times higher than those for the cast alloys (< 200%). Maximum ductility is observed in the UFG alloys with Sc:Zr = 0.28–0.32 (in at.%). Strain rate sensitivity coefficient of flow stress m is close to 0.4 at 450–500 °C and do not depend on Sc:Zr ratio.

2. Under superplastic deformation of UFG Al-6%Mg-Sc-Zr alloys, intense pore formation is observed, and an increase in Sc content in the alloys increases the volume fraction and size of pores. The pores are found mainly along grain boundaries of the aluminum alloys. It was suggested that intense pore formation results from large Al_3Sc particles that are formed by discontinuous precipitation.

3. Under superplastic deformation of the UFG alloys, dynamic recrystallization occurs accompanied by the formation of a homogeneous fine-grained microstructure in the deformed part of the specimens. The average grain size in the deformed part of the specimens decreases while Sc content in Al-6%Mg-Sc-Zr alloys increases. Microstructure of the UFG alloys with high Zr content after superplastic deformation is characterized by abnormally coarse grains with pores along their boundaries.

Author Contributions: Conceptualization, V.C. and A.N.; methodology, V.C.; validation, V.C., A.N. and O.P.; formal analysis, V.C. and O.P.; investigation, M.G., S.S., K.L., G.N., M.C., A.B., V.K.; resources, V.C.; data curation, A.N.; writing—original draft preparation, V.C., A.N. and O.P.; writing—review and editing, V.C., A.N. and O.P.; visualization, A.N. and O.P..; supervision, V.C.; project administration, V.C.; funding acquisition, V.C. All authors have read and agreed to the published version of the manuscript.

Funding: This research was funded by Russian Science Foundation, grant number 22-13-00149.

Data Availability Statement: Not applicable.

Acknowledgments: Authors thank V.V. Zakharov (Russian Institute of Light Alloys (VILS), Moscow, Russia) for recommendations on the choice of the compositions and casting regimes of the Al alloys.

Conflicts of Interest: The authors declare no conflict of interest.

References

1. Hirsch, J. Recent development in aluminium for automotive applications. *Transactions of Nonferrous Metals Society of China* **2014**, *24*, 1995-2002. doi:10.1016/S1003-6326(14)63305-7
2. Fan, L.; Ma, J.; Zou, C. et al. Revealing foundations of the intergranular corrosion of 5XXX and 6XXX Al alloys. *Materials Letters* **2020**, *271*, 127767. doi:10.1016/j.matlet.2020.127767
3. Huskins, E.L.; Cao, B.; Ramesh, K.T. Strengthening mechanisms in anal-Mg alloy. *Materials Science and Engineering A* **2010**, *527*, 1292-1298. doi:10.1016/j.msea.2009.11.056
4. Zheng, K.; Politis, D.J.; Wang, L.; Lin, J. A review of forming techniques for manufacturing lightweight complex-shaped aluminium panel components. *International Journal of Lightweight Materials and Manufacture* **2018**, *1*, 55-80. doi:10.1016/j.ijlmm.2018.03.006
5. Miller, W.S.; Zhuang, L.; Bottema, J. et al. Recent development in aluminium alloys for the automotive industry. *Materials Science and Engineering A* **2000**, *280*, 37-49. doi:10.1016/S0921-5093(99)00653-X
6. Wahid, M.A.; Siddiquee, A.N.; Khan, Z.A. Aluminum alloys in marine construction: characteristics, applications, and problems from a fabrication viewpoint. *Marine Systems & Ocean Technology* **2020**, *15*, 70-80. https://doi.org/10.1007/s40868-019-00069-w
7. Kasen, S.D.; Tubbs, D. Strength degradation in AA5083 armor plate after exposure to elevated temperatures. *Journal of Engineering Materials and Technology* **2023**, *145*, 011001. doi:10.1115/1.4055052

8. Lloyd, D.J. The deformation of commercial aluminium-magnesium alloys. *Metallurgical Transactions A* **1980**, *11*, 1287-1294. doi:10.1007/BF02653482
9. Yan, J.; Heckman, N.M.; Velasco, L.; Hodge, A.M. Improve sensitization and corrosion resistance of an Al-Mg alloy by optimization of grain boundaries. *Scientific Reports* **2016**, *6*, 26870. doi:10.1038/srep26870
10. Singh, V.P.; Patel, S.K.; Ranjan, A.; Kuriachen, B. Recent research progress in solid state friction-stir welding of aluminium-magnesium alloys: a critical review. *Journal of Materials Research and Technology* **2020**, *9*, 6217-6256. doi:10.1016/j.jmrt.2020.01.008
11. Rabinovich, M.Kh.; Kudryashov, V.G.; Markushev, M.V. Effect of grain size on the structural strength of the aluminum alloy AMg6. *Metal Science and Heat Treatment* **1988**, *30*, 609-612. doi:10.1007/BF00778267
12. Røyset, J.; Ryum, N. Scandium in aluminium alloys. *International Materials Reviews* **2005**, *50*, 19-44. doi:10.1179/174328005X14311
13. Yelagin, V.I.; Shvechkov, Ye.I.; Filatov, Yu.A.; Zakharov, V.V. Crack resistance of Al-Mg-Sc alloy sheets. *Light Alloy Technology* **2005**, *1-4*, 40-44. (in Russian). https://www.elibrary.ru/item.asp?id=12379194
14. Filatov, Yu.A.; Plotnikov, A.D. A structure and properties of wrought 01570C Al-Mg-Sc aluminium alloy semiproducts. *Light Alloy Technology* **2011**, *2*, 15-26. (in Russian). https://www.elibrary.ru/item.asp?id=18772656
15. Davydov, V.G.; Yelagin, V.I.; Zakharov, V.V.; Filatov, Yu.A. On the prospects of application of new 01570 high-strength weldable Al-Mg-Sc alloy in aircraft industry. *Materials Science Forum* **1996**, *217-222*, 1841-1846. doi:10.4028/www.scientific.net/msf.217-222.1841
16. Toropova, L.S.; Eskin, D.G.; Kharakterova, M.L.; Dobatkina, T.V. *Advanced aluminum alloys containing scandium: Structure and properties*. Taylor and Francis Group: London, UK, 2017, 175 p. doi:10.4324/9781315097541
17. Filatov, Yu.A. Deformable alloys based on the Al-Mg-Sc system. *Metal Science and Heat Treatment* **1996**, *38*, 271-274. doi:10.1007/bf01395830
18. Davydov, V.G.; Rostova, T.D.; Zakharov, V.V.; Filatov, Yu.A.; Yelagin, V.I. Scientific principles of making an alloying addition of scandium to aluminium alloys. *Materials Science and Engineering A* **2000**, *280*, 30-36. doi:10.1016/S0921-5093(99)00652-8
19. Filatov, Yu.A.; Yelagin, V.I.; Zakharov, V.V. New Al-Mg-Sc alloys. *Materials Science and Engineering A* **2000**, *280*, 97-101. doi:10.1016/S0921-5093(99)00673-5
20. Filatov, Yu.A. Al-Mg-Sc systems for welded and brazed constructions. *Tsventnye Metally* **2014**, *1*, 80-86.
21. Shvechnikov, E.I.; Filatov, Yu.A.; Zakharov, V.V. Mechanical and life properties of sheets from the alloys of the Al-Mg-Sc systems. *Metals Science and Heat Treatment* **2017**, *59*, 454-462. doi:10.1007/s11041-017-0171-4
22. Filatov, Yu.A., Baidin, N.G.; Dobrozhinskaya, R.I.; Khamnagdayeva, Ye.A., Ovsyannikov, B.V. A new 1545K Al-Mg-Sc system-based nonheat-treatable weldable cryogenic alloy. *Light Alloy Technology* **2014**, *1*, 32-36. (in Russian). https://www.elibrary.ru/item.asp?id=21815646
23. Zakharov, V.V.; Filatov, Yu.A. Modern trends in the development of aluminum alloys doped with scandium. *Light Alloy Technology* **2022**, *3*, 9-18. (in Russian). doi:10.24412/0321-4664-2022-3-9-18
24. Filatov, Yu.A. Further development of Al-Mg-Sc wrought alloys. *Light Alloy Technology* **2021**, *2*, 12-22. (in Russian). doi:10.24412/0321-4664-2021-2-12-22
25. Filatov, Yu.A.; Snegiryova, L.A. Mechanical properties and thermal conductivity of rods extruded from 01513 (Al-Mg-Sc-Hf) and 01407 (Al-Sc-Zr) aluminum alloys. *Light Alloy Technology* **2020**, *3*, 34-38. (in Russian). https://www.elibrary.ru/item.asp?id=44408062
26. Filatov, Yu.A. Research works undertaken at VILS in the field of Al-Mg-Sc wrought alloys. History of development, structure, properties, applications, problems and prospects. *Light Alloy Technology* **2017**, *3*, 7-24. (in Russian). https://www.elibrary.ru/item.asp?id=30507255
27. Baydin, N.G.; Filatov, Yu.A. Al-Mg-Mn-Sc-Zr-Gd (01570-type) alloy cost effectively alloyed with scandium. *Light Alloy Technology* **2017**, *3*, 45-51. https://www.elibrary.ru/item.asp?id=30507259
28. Baydin, N.G.; Filatov, Yu.A. A structure and mechanical properties of sheets in 01570-type aluminium alloy with lower scandium content. *Light Alloy Technology* **2016**, *4*, 12-17. https://www.elibrary.ru/item.asp?id=28884338
29. Davydov, V.G.; Elagin, V.I.; Zakharov, V.V.; Rostova, D. Alloying aluminum alloys with scandium and zirconium additives. *Metal Science and Heat Treatment* **1996**, *38*, 347-352. doi:10.1007/bf01395323
30. Elagin, V.I.; Zakharov, V.V.; Rostova, D. Scadium-alloyed aluminum alloys. *Metal Science and Heat Treatment* **1992**, *34*, 37-45. doi:10.1007/BF00768707
31. Konstantinov, I.L.; Yuryev, P.O., Baranov, V.N. et al. Study the influence of scandium content and annealing regimes on the properties of alloys 1580 and 1581. *International Journal of Lightweight Materials and Manufacture* **2023**, *6*, 15-24. doi:10.1016/j.ijlmm.2022.09.002
32. Zakharov, V.V.; Fisenko, I.A. Alloying aluminum alloys with scandium. *Metal Science and Heat Treatment* **2017**, *59*, 278-284. doi:10.1007/s11041-017-0142-9
33. Zakharov, V.V.; Fisenko, I.A. Some principles of alloying of aluminum alloys with scandium and zirconium in ingot production of deformed semiproducts. *Metal Science and Heat Treatment* **2019**, *61*, 217-221. doi:10.1007/s11041-019-00403-4
34. Zha, M.; Tian, T.; Jia, H.-L. et al. Sc/Zr ratio-dependent mechanisms of strength evolution and microstructural thermal stability of multi-scale heterostructured Al-Mg-Sc-Zr alloy. *Journal of Materials Science and Technology* **2023**, *140*, 67-78. doi:10.1016/j.jmst.2022.09.009
35. Jiang, F.; Zhou, J.; Huang, H.; Qu, J. Characterisation of microstructure and mechanical properties in Al-Mg alloy with addition of Sc and Zr. *Materials Research Innovation* **2014**, *18*, S4-228-S4-234. doi:10.1179/1432891714Z.000000000686

36. Nieh, T.G.; Kaibyshev, R.; Hsiung, L.M. et al. Subgrain formation and evolution during the deformation of an Al-Mg-Sc alloy at elevated temperatures. *Scripta Materialia* **1997**, *36*, 1011-1016. doi:10.1016/S1359-6462(96)00479-4
37. Kaibyshev, R.; Musin, F.; Avtokratova, E.; Motohashi, Y. Deformation behavior of a modified 5083 aluminium alloy. *Materials Science and Engineering A* **2005**, *392*, 373-379. doi:10.1016/j.msea.2004.10.002
38. Vertano, J.S.; Bruemmer, S.M.; Pawloski, L.M.; Robertson, I.M. Influence of the particle size on recrystallization and grain growth in Al-Mg-X alloys. *Materials Science and Engineering A* **1997**, *238*, 101-107. doi:10.1016/S0921-5093(97)00445-0
39. Li, M.; Pan, Q.; Shi, Y. et al. High strain rate superplasticity in an Al-Mg-Sc-Zr alloy processed via simple rolling. *Materials Science and Engineering A* **2017**, *687*, 298-305. doi:10.1016/j.msea.2017.01.091
40. Mikhaylovskaya, A.V.; Kishchik, A.A.; Kotov, A.D. et al. Precipitation behavior and high strain rate superplasticity in a novel fine-grained aluminum based alloy. *Materials Science and Engineering A* **2019**, *760*, 37-46. doi:10.1016/j.msea.2019.05.099
41. Nieh, T.G.; Hsiung, L.M.; Wadsworth, J.; Kaibyshev, R. High strain rate superplasticity in a continuously recrystallized Al-6%Mg-0.3%Sc alloy. *Acta Materialia* **1998**, *46*, 2789-2800. doi:10.1016/S1359-6454(97)00452-7
42. Bhatta, L.; Pesin, A.; Zhilyaev, A. et al. Recent development of superplasticity in aluminum alloys: A review. *Metals* **2020**, *10*, 77. doi:10.3390/met10010077
43. Kaibyshev, R.; Avtokratova, E.; Apollonov, A.; Davies, R. High strain rate superplasticity in an Al-Mg-Sc-Zr alloy subjected to simple thermomechanical processing. *Scripta Materialia* **2006**, *54*, 2119-2124. doi:10.1016/j.scriptamat.2006.03.020
44. Portnoy, V.K.; Yakovtseva, O.A.; Kishchik, A.A. et al. Use the heterogenization for improving alloy AA5083 superplasticity indices. *Metallurgist* **2018**, *62*, 449-455. doi:10.1007/s11015-018-0680-4
45. Mikhaylovskaya, A.V.; Kotov, A.D.; Kishchik, M.S. et al. The effect of isothermal multi-direction forging on the grain structure, superplasticity, and mechanical properties of the conventional Al-Mg-based alloy. *Metals* **2019**, *9*, 33. doi:10.3390/met9010033
46. Kishchik, A.A.; Mikhaylovskaya, A.V.; Levchenko, V.S.; Portnoy, V.K. Formation of microstructure and the superplasticity of Al-Mg-based alloy. *Physics of Metals and Metallography* **2017**, *118*, 96-103. doi:10.1134/S0031918X16120085
47. Kishchik, M.S.; Mikhaylovskaya, A.V.; Levchenko, V.S. et al. Formation of fine-grained structure and superplasticity in commercial aluminum alloy 1565ch. *Metal Science and Heat Treatment* **2017**, *58*, 543-547. doi:10.1007/s11041-017-0051-y
48. Mikhaylovskaya, A.V.; Yakovtseva, O.A.; Mochugovskiy, A.G. et al. Influence of minor Zn addition on grain boundary anelasticity, grain boundary sliding, and superplasticity of Al-Mg-based alloys. *Journal of Alloys and Compounds* **2022**, *926*, 166785. doi:10.1016/j.jallcom.2022.166785
49. Yakovtseva, O.A.; Kishchik, A.A.; Cheverikin, V.V. et al. The mechanisms of the high-strain-rate superplastic deformation of Al-Mg-based alloy. *Materials Letters* **2022**, *325*, 132883. doi:10.1016/j.matlet.2022.132883
50. Porntoy, V.K.; Rylov, D.S., Levchenko, V.S.; Mikhaylovskaya, A.V. The influence of chromium on the structure and superplasticity of Al-Mg-Mn alloy. *Journal of Alloys and Compounds* **2013**, *581*, 313-317. doi:10.1016/j.jallcom.2013.07.075
51. Mochugovskiy, A.G.; Mikhaylovskaya, A.V.; Zadorognyy, M.Yu.; Golovin, I.S. Effect of heat treatment on the grain size control, superplasticity, internal friction, ana mechanical properties of zirconium-bearing aluminum-based alloy. *Journal of Alloys and Compounds* **2021**, *856*, 157455. doi:10.1016/j.jallcom.2020.157455
52. Kotov, A.D.; Mochugovskiy, A.G.; Mosleh, A.O. et al. Microstructure, superplasticity, and mechanical properties of Al-Mg-Er-Zr alloys. *Materials Charaterization* **2022**, *186*, 111825. https://doi.org/10.1016/j.matchar.2022.111825
53. Nie, Z.-R.; Jin, T.-N.; Zou, J.-X. et al. Development on research of advanced rare-earth aluminum alloy. *Transactions of Nonferrous Metals Society of China* **2003**, *13*, 50-514.
54. Pozdnyakov, A.V.; Osipenkova, A.A.; Popov, D.A.; Makhov, S.V.; Napalkov, V.I. Effect of low additions of Y, Sm, Gd, Hf and Er on the structure and hardness of alloy Al-0.2%Zr-0.1%Sc. *Metal Science and Heat Treatment* **2017**, *58*, 537–542, doi:10.1007/s11041-017-0050-z
55. Wen, S.P.; Gao, K.Y.; Huang, H.; Wang, W.; Nie, Z.R. Role of Yb and Si on the precipitation hardening and recrystallization of dilute Al-Zr alloy. *J. Alloys Compd.* **2014**, *599*, 65–70, doi:10.1016/j.jallcom.2014.02.065.
56. Wen, S.P.; Gao, K.Y.; Li, Y.; Huang, H.; Nie, Z.R. Synergetic effect of Er and Zr on the precipitation hardening of Al-Er-Zr alloy. *Scr. Mater.* **2011**, *65*, 592–595, doi:10.1016/j.scriptamat.2011.06.033.
57. Voroshilov, D.S.; Motkov, M.M.; Sidelnikov, S.B.; Sokolov, S.E.; Durnopyanov, A.V.; Konstantinov, I.L.; Bespalov, V.M.; Bermeshev, T.V.; Gudkov, I.S.; Voroshilova, M.V.; Mansurov, Y.N.; Berngardt, V.A. Obtaining Al-Zr-Hf wire using electromagnetic casting, combined rolling-extrusion, and drawing. *Int. J. Lightweight Mater. Manufacture* **2022**, *5*, 352-368. doi:10.1016/j.ijlmm.2022.04.002
58. Zhou, T.; Xie, H.; Jiang, Z. Mechanical and electrical properties of Y-containing Al-Zr heat-resistant alloy produced by dynamic ECAE process. *J. Wuhan Univ. Techn.* **2022**, *37*, 123-129. 10.1007/s11595-022-2508-0
59. Li, H.; Bin, J.; Liu, J.; Gao, Z.; Lu, X. Precipitation evolution and coarsening resistance at 400 °C of Al microalloyed with Zr and Er. *Scr. Mater.* **2012**, *67*, 73-76. 10.1016/j.scriptamat.2012.03.026
60. Kang, W.; Li, H.Y.; Zhao, S.X.; Han, Y.; Yang, C.L.; Ma, G. Effects of homogenization treatments on the microstructure evolution, microhardness and electrical conductivity of dilute Al-Sc-Zr-Er alloys. *J. Alloys Compd.* **2017**, *704*, 683-692. 10.1016/j.jallcom.2017.02.043
61. Mochegovskiy, A.G.; Mikhaylovskaya, A.V.; Tabachkova, N.Yu.; Portnoy, V.K. The mechanism of $L1_2$ precipitation, microstructure and tensile properties of Al-Mg-Er-Zr alloy. *Mater. Sci. Eng. A* **2019**, *744*, 195-205. doi:10.1016/j.msea.2018.11.135
62. Gao, Z.; Li, H.; Liu, J.;Lu, X.; Ou, Y. Effects of ytterbium and zirconium on precipitation evolution and coarsening resistance in aluminum during isothermal aging. *J. Alloys Compd.* **2014**, *592*, 100-104. 10.1016/j.jallcom.2014.01.009

63. Wu, H.; Wen, S.P.; Wu, X.L.; Gao, K.Y.; Huang, H.; Wang, W.; Nie, Z.R. A study of precipitation strengthening and recrystallization behavior in dilute Al-Er-Hf-Zr alloys. *Mater. Sci. Eng. A*. **2015**, *639*, 307-313. doi:10.1016/j.msea.2015.05.027
64. Gao, H.; Feng, W.; Gu, J.; Wang, J.; Sun, B. Aging and recrystallization behavior of precipitation strengthened Al-0.25Zr-0.03Y alloy. *J. Alloys Compd.* **2017**, *696*, 1039-1045. 10.1016/j.jallcom.2016.12.064
65. Zhang, Y.; Zhou, W.; Gao, H.; Han, Y.; Wang, K.; Wang, J.; Sun, B.; Gu, S.; You, W. Precipitation evolution of Al-Zr-Yb alloys during isochronal aging. *Scr. Mater.* **2013**, *69*, 477-480. doi:10.1016/j.scriptamat.2013.06.003
66. Mochegovskiy, A.G.; Barkov, R.Yu.; Mikhaylovskaya, A.V.; Loginova, L.S.; Yakovtseva, O.A.; Pozdniakov, A.V. Structure and properties of Al-4.5Mg-0.15Zr compositions alloyed with Er, Y, and Yb. *Phys. Metals Metallogr.* **2022**, *123*, 466-473. doi:10.1134/S0031918X22050088
67. Gao, H.; Wang, Y.; Wang, J.; Sun, B.; Apelian, D. Aging and recrystallization behavior of quaternary Al-0.25Zr-0.03Y-0.10Si alloy. *Mater. Sci. Eng. A* **2019**, *763*, 138160. 10.1016/j.msea.2019.138160
68. Pozdniakov, A.V.; Barkov, R.Yu.; Prosviryakov, A.S.; Churyumov, A.Yu.; Golovin, I.S.; Zolotorevskiy, V.S. Effect of Zr on the microstructure, recrystallization behavior, mechanical properties and electrical conductivity of the novel Al-Er-Y alloy. *J. Alloys Compd.* **2018**, *765*, 1-6. doi:10.1016/j.jallcom.2018.06.163
69. Nokhrin, A.; Shadrina, I.; Chuvil'deev, V.; Kopylov, V. Study of structure and mechanical properties of fine-grained aluminum alloys Al-0.6wt.%Mg-Zr-Sc with ratio Zr:Sc = 1.5 obtained by cold drawing. *Materials* **2019**, *12*, 316. doi:10.3390/ma12020316
70. Nokhrin, A.V.; Shadrina, I.S.; Chuvil'deev, V.N.; Kopylov, V.I.; Berendeev, N.N.; Murashov, A.A.; Bobrov, A.A.; Tabachkova, N.Yu.; Smirnova, E.S.; Faddeev, M.A. Investigation of thermal stability of microstructure and mechanical properties of bimetallic fine–grained wires from Al–0.25%Zr–(Sc,Hf) alloys. *Materials* **2022**, *15*, 185. doi:10.3390/ma15010185
71. Booth-Morrison, C.; Dunand, D.C.; Seidman, D.N. Coarsening resistance at 400 °C pf precipitation-strengthened Al-Zr-Sc-Er alloys. *Acta Mater.* **2011**, *59*, 7029-7042. doi:10.1016/j.actamat.2011.07.057
72. Gorlov, L.E.; Loginova, I.S.; Glavatskikh, M.V.; Barkov, R.Yu.; Pozdniakov, A.V. Novel precipitation strengthened Al-Y-Sc-Er alloy with high mechanical properties, ductility and electrical conductivity produced by different thermomechanical treatments. *J. Alloys Compd.* **2022**, *918*, 165748. doi:10.1016/j.jallcom.2022.165748
73. Barkov, R.Yu.; Mikhaylovskaya, A.V.; Yakovtseva, O.A.; Loginova, I.S.; Prosviryakov, A.S.; Pozdniakov, A.V. Effects of thermomechanical treatment on the microstructure, precipitation strengthening, internal friction, and thermal stability of Al-Er-Yb-Sc alloys with good electrical conductivity. *J. Alloys Compd.* **2021**, *855*, 157367. doi:10.1016/j.jallcom.2020.157367
74. Barkov, R.Yu.; Yakovtseva, O.A.; Mamzurina, O.I.; Loginova, I.S.; Medvedeva, S.V.; Prosviryakov, A.S.; Mikhaylovskaya, A.V., Pozdniakov, A.V. Effect of Yb on the structure and properties of an electroconductive Al-Y-Sc alloy. *Phys. Metals Metallogr.* **2020**, *121*, 604-609. doi:10.1134/S0031918X20060022
75. Tang, C.-I.; Zhou, D.-J. Precipitation hardening behavior of dilute binary Al-Yb alloy. *Transact. Nonferr. Met. Soc. China* **2014**, *24*, 2326-2330. doi:10.1016/S1003-6326(14)63352-5
76. Wu, H.; Zhang, Q.; Li, L.; Huang, M.; Zheng, Z.; Wen, S. Thermal stability of the precipitates in dilute Al-Er-Zr/Hf alloys at elevated temperatures. *Metals* **2022**, *12*, 1242. doi:10.3390/met12081242
77. Nes, E.; Ryum, N. On the formation of fan-shaped precipitates during the decomposition of a highly supersaturated Al-Zr solid solution. *Scripta Materialia* **1971**, *5*, 987-989. doi:10.1016/0036-9748(71)90142-6
78. Nes, E.; Billdal, H. The mechanism of discontinuous precipitation of the metastable Al_3Zr phase from an Al-Zr solid solution. *Acta Metall.* **1977**, *25*, 1039-1046. doi:10.1016/0001-6160(77)90133-X
79. Mikhaylovskaya, A.V.; Mochugovskiy, A.G.; Levchenko, V.S.; Tabachkova, N.Yu.; Mufalo, W.; Portnoy, V.K. Precipitation behavior of $L1_2$ Al_3Zr phase in Al-Mg-Zr alloy. *Materials Charaterization* **2018**, *139*, 30-37. doi:10.1016/j.matchar.2018.02.030
80. Mochugovskiy, A.G.; Mikhaylovskaya, A.V. Comparison of precipitation kinetics and mechanical properties in Zr and Sc-bearing aluminum-based alloys. *Material Letters* **2020**, *275*, 128096. doi:10.1016/j.matlet.2020.128096
81. Chuvil'deev; V.N.; Shadrina, Ya.S.; Nokhrin, A.V.; Kopylov, V.I.; Bobrov, A.A.; Gryaznov, M.Yu.; Shotin, S.V.; Tabachkova, N.Yu.; Chegurov, M.K.; Melekhin, N.V. An investigation of thermal stability of structure and mechanical properties of Al-0.5Mg-Sc ultrafine-grained aluminum alloys. *Journal of Alloys and Compounds* **2020**, *831*, 154805. doi:10.1016/j.jallcom.2020.154805
82. Chuvil'deev, V.N.; Gryaznov, M.Yu.; Shotin, S.V.; Kopylov, V.I.; Nokhrin, A.V.; Likhnitskii, C.V.; Chegurov, M.K.; Bobrov, A.A.; Tabachkova, N.Yu.; Pirozhnikova, O.E. Investigation of superplasticity and dynamic grain growth in ultrafine-grained Al-0.5%Mg-Sc alloys. *Journal of Alloys and Compounds* **2021**, *877*, 160099. doi:10.1016/j.jallcom.2021.160099
83. Gryaznov; M.Yu.; Shotin, S.V.; Nokhrin, A.V. et al. Investigation of effect of preliminary annealing on superplasticity of ultrafine-grained conductor aluminum alloys Al-0.5%Mg-Sc. *Materials* **2022**, *15*, 176. doi:10.3390/ma15010176
84. Komura, S.; Berbon, P.B.; Furukawa, M.; Horita, Z.; Nemoto, M.; Langdon, T.G. High strain rate superplasticity in an Al-Mg alloy containing scandium. *Scripta Materialia* **1998**, *38*, 1851-1856. doi:10.1016/S1359-6462(98)00099-2
85. Musin, F.; Kaibyshev, R.; Motohashi, Y.; Itoh, G. High strain rate superplasticity in a commercial Al-Mg-Sc alloy. *Scripta Materialia* **2004**, *50*, 511-516. doi:10.1016/j.scriptamat.2003.10.021
86. Lee, S.; Utsunomiya, A.; Akamatsu, H.; Neishi, K.; Furukawa, M.; Horita, Z.; Langdon, T.G. Influence of scandium and zirconium on grain stability and superplastic ductilities in ultrafine-grained Al-Mg alloys. *Acta Materialia* **2002**, *50*, 553-564. doi:10.1016/S1359-6454(01)00368-8
87. Komura, S.; Horita, Z.; Furukawa, M.; Nemoto, M.; Langdon, T.G. Influence of scandium on superplastic ductilities in an Al-Mg-Sc alloy. *Journal of Materials Research* **2000**, *15*, 2571-2576. doi:10.1557/JMR.2000.0367
88. Ma, Z.Y.; Mishra, R.S. Development of ultrafine-grained microstructure and low temperature (0.48 T_m) superplasticity in friction stir processed Al-Mg-Zr. *Scripta Materialia* **2005**, *53*, 75-80. doi:10.1016/j.scriptamat.2005.03.018

89. Liu, F.C.; Ma, Z.Y.; Chen, L.Q. Low-temperature superplasticity of Al-Mg-Sc alloy produced by friction stir processing. *Scripta Materialia* **2009**, *60*, 968-971. doi:10.1016/j.scriptamat.2009.02.021
90. Liu, F.C.; Ma, Z.Y. Contribution of grain boundary sliding in low-temperature superplasticity of ultrafine-grained aluminum alloys. *Scripta Materialia* **2010**, *62*, 125-128. doi:10.1016/j.scriptamat.2009.10.010
91. Avtokratova, E.; Sitdikov, O.; Markushev, M.; Mulyukov, R. Extraordinary high-strain rate superplasticity of severely deformed Al-Mg-Sc-Zr alloy. *Materials Science and Engineering A* **2012**, *538*, 386-390. doi:10.1016/j.msea.2012.01.041
92. Liu, F.C.; Xue, P.; Ma, Z.Y. Microstructural evolution in recrystallized and unrecrystallized Al-Mg-Sc alloys during superplastic deformation. *Materials Science and Engineering A* **2012**, *547*, 55-63. doi:10.1016/j.msea.2012.03.076
93. Mikhaylovskaya, A.V.; Yakovtseva, O.A.; Golovin, I.S. et al. Superplastic deformation mechanisms in fine-grained Al-Mg based alloys. *Materials Science and Engineering A* **2015**, *627*, 31-41. doi:10.1016/j.msea.2014.12.099
94. Ma, Z.Y.; Mishra, R.S.; Mahoney, M.W.; Grimes, R. Effect of friction stir processing on the kinetics of superplastic deformation in an Al-Mg-Zr alloy. *Metallurgical and Materials Transactions A* **2005**, *36*, 1447-1458. doi:10.1007/s11661-005-0237-6
95. Li, M.; Pan, Q.; Shi, Y. et al. High strain rate superplasticity in an Al-Mg-Sc-Zr alloy processed via simple rolling. *Materials Science and Engineering A* **2017**, *687*, 298-305. doi:10.1016/j.msea.2017.01.091
96. Mikhaylovskaya, A.V.; Yakovtseva, O.A.; Cheverikin, V.V. et al. Superplastic behavior of Al-Mg-Zn-Zr-Sc-based alloys at high strain rate. *Materials Science and Engineering A* **2016**, *659*, 225-233. doi:10.1016/j.msea.2016.02.061
97. Xu, G.; Cao, X.; Zhang, T. et al. Achieving high strain rate superplasticity of an Al-Mg-Sc-Zr alloy by a new asymmetrical rolling technology. *Materials Science and Engineering A* **2016**, *672*, 98-107. doi:10.1016/j.msea.2016.06.070
98. Turba, K.; Málek, P.; Cieslar, M. Superplasticity in an Al-Mg-Sc-Zr alloy produced by equal-channel angular pressing. *Materials Science and Engineering A* **2007**, *462*, 91-94. doi:10.1016/j.msea.2006.01.178
99. Rabinovich, M.Kh., Markushev, M.V. Influence of fine-grained structure and superplastic deformation on the strength of aluminium alloys. *Journal of Materials Science* **1996**, *31*, 4997-5001. doi:10.1007/BF00355893
100. Maeng, D.Y.; Lee, J.H.; Hong, S.I. The effect of transition elements on the superplastic behavior of Al-Mg alloys. *Materials Science and Engineering A* **2003**, *357*, 188-195. doi:10.1016/S0921-5093(03)00160-6
101. Yuzbekova, D.; Mogucheva, A.; Kaibyshev, R. Superplasticity of ultrafine-grained Al-Mg-Sc-Zr alloy. *Materials Science and Engineering* **2016,** *675*, 228-242. doi:10.1016/j.msea.2016.08.074
102. Duan, Y.; Xu, G.; Tang, L. et al. Excellent high strain rate superplasticity of Al-Mg-Sc-Zr alloy sheet produced by an improved asymmetrical rolling process. *Journal of Alloys and Compounds* **2017**, *715*, 311-321. doi:10.1016/j.jallcom.2017.04.273
103. Musin, F.; Kaibyshev, R.; Motohashi, Y.; Itoh, G. Superplastic behavior and microstructure evolution in a commercial Al-Mg-Sc alloy subjected to intense plastic deformation. *Metallurgical and Materials Transactions A* **2004**, *35*, 2383-2392. doi:10.1007/s11661-006-0218-4
104. Bobruk, E.V.; Safargalina, Z.A.; Golubev, O.V.; Baykov, D.; Kazykhanov, V.U. The effect of ultrafine-grained states on superplastic behavior of Al-Mg-Si alloy. *Materials Letters* **2019**, *255*, 126503. doi:10.1016/j.matlet.2019.126503
105. Duan, Y.-I.; Qian, J.; Xiao, D. et al. Effect of Sc and Er additions on superplastic ductilities in Al-Mg-Mn-Zr alloy. *Journal of Central South University* **2016**, *23*, 1283-1292. doi:10.1007/s11771-016-3178-x
106. Sitdikov, O.S.; Garipova, R.N.; Avtokratova, E.V. et al. Structural changes during severe hot forging of the aluminum alloy 1570C. *Letters on Materials* **2016**, *6*, 200-204. doi:10.22226/2410-3535-2016-3-200-204
107. Zhang, C.; Xiao. Y.; Ma, K. et al. Superplastic flow and deformation mechanism of the rolled Al-Mg-Li-Sc-Zr alloy with banded microstructure. *Metals* **2021**, *11*, 404. doi:10.3390/met11030404
108. Sitdikov, O., Avtokratova, E.; Latypova, O., Markushev, M. Structure and superplasticity of the Al-Mg-TM alloy after Equal Channel Angular Pressing and rolling. *Letters on Materials* **2018**, *8*, 561-566. doi:10.22226/2410-3535-2018-4-561-566
109. Chuvil'deev, V.N.; Kopylov, V.I.; Gryaznov, M.Yu. et al. Doubling of strength and plasticity of a commercial aluminum-based alloy (AMg6) processed by Equal Channel Angular Pressing. *Doklady Physics* **2008**, *53*, 584-587. doi:10.1134/S1028335808110086
110. Chuvil'deev; V.N.; Gryaznov, M.Yu.; Kopylov, V.I. et al. Superplasticity of the Al-18%Si microcrystalline hypereutectic alloy. *Doklady Physics* **2008**, *53*, 148-151. doi:10.1134/S1028335808030087
111. Nieh, T.G.; Wadsworth, J.; Sherby, O.D. *Superplasticity in Metals and Ceramics*, Cambridge University Press: Cambridge, UK, 1997.
112. Novikov, I.I.; Portnoy, V.K. *Superplasticity of fine-grained alloys*, Metallurgiya: Moscow, USSR, 1981 (in Russian).
113. Perevezentsev, V.N.; Rybin, V.V.; Chuvil'deev, V.N. The theory of structural superplasticity: I. The physical nature of the superplasticity phenomenon. *Acta Metallurgica et Materialia* **1992**, *40*, 887-894. doi:10.1016/0956-7151(92)90065-M
114. Chuvil'deev; V.N.; Shavleva, A.V.; Nokhrin, A.V., et al. Influence of the grain size and structural state of grain boundaries on the parameter of low-temperature and high-rate superplasticity of nanocrystalline and microcrystalline alloys. *Physics of the Solid State* **2010**, *52*, 1098-1106. doi:10.1134/S1063783410050422
115. Segal, V.M.; Beyerlein, I.J.; Tome, C.N.; Chuvil'deev, V.N.; Kopylov, V.I. *Fundamentals and Engineering of Severe Plastic Deformation*. Nova Science Publishers: New York, US, 2010, 542 p.
116. Segal, V. Review: Modes and process of severe plastic deformation. *Materials* **2018**, *11*, 1175. doi:10.3390/ma11071175
117. Segal, V. Equal-channel angular extrusion (ECAE): From a laboratory curiosity to an industrial technology. *Metals* **2020**, *10*, 244. doi:10.3390/met10020244
118. Novikov, I.I.; Portnoy, V.K.; Titov, A.O.; Belov, D.Yu. Dynamic recrystallization at superplastic deformation of duraluminum with initial recrystallized structure. *Scripta Materialia* **2000**, *42*, 899-904. doi:10.1016/S1359-6462(00)00310-9

119. Chuvil'deev, V.N.; Nokhrin, A.V.; Kopylov, V.I. et al. Investigation of mechanical properties and corrosion resistance of fine-grained aluminum alloys Al-Zn with reduced zinc content. *Journal of Alloys and Compounds* **2022**, *891*, 162110.
120. Perevezentsev, V.N.; Rybin, V.V.; Chuvil'deev, V.N. The theory of structural superplasticity: IV. Cavitation during superplastic deformation. *Acta Metallurgica et Materialia* **1992**, *40*, 915-923. doi:10.1016/0956-7151(92)90068-P
121. Rybin, V.V.; Perevezentsev, V.N.; Chuvil'deev, V.N. Pore nucleation at the precipitate-matrix interface under superplastic deformation. *Surface* **1986**, *11*, 130-139. (in Russian).
122. *Kristallisation aus Schmelzen*. Eds. Hein, K. and Buhrig. Vew Deutscher Verlag Für Grundstoffindustrie: E. Leipzig, Germany, 1983, 356 p. (in Germany).
123. Harada, Y.; Dunand, D.C. Microstructure of Al_3Sc with ternary rare-earth additions. *Intermetallics* **2009**, *17*, 17-24. doi:10.1016/j.intermet.2008.09.002
124. Berezina, A.L.; Monastyrska, T.O.; Molebny, O.A.; Nosenko, V.K.; Kotko, A.V. Decomposition processes in the anomalous supersaturated solid solution of binary and ternary aluminium alloys alloyed with Sc and Zr. *Acta Physica Polonica A* **2012**, *122*, 539-543. doi:10.12693/APhysPolA.122.539
125. Monastyrska, T.O.; Berezina, A.L.; Molebny, O.A.; Kotko, A.V. Effect of alloying with transitions metals on the aging of anomalous supersaturated solid solution of Al-Mg alloys. *Applied Nanoscience* **2022**, *12*, 513-522. doi:10.1007/s13204-021-01705-x
126. Xue, C.; Wang, Y.; Wang, J. Designing elastic modulus of Al_3X precipitates in Al alloys by identifying effective atom bonds and stabilizing coherent structure. *Journal of Alloys and Compounds* **2022**, *896*, 162619. doi:10.1016/j.jallcom.2021.162619
127. Bakare, F.; Babalola, M.I.; Lyorzor, B.E. The role of alloying elements on the structural, mechanical and thermodynamics properties of Al_3X binary alloy system (X = Mg, Sc and Zr): first principle calculations. *Materials Research Express* **2017**, *4*, 116502. doi:10.1088/2053-1591/aa9485
128. Senkov, O.N.; Shagiev, M.R.; Senkova, S.V.; Miracle, D.B. Precipitation of $Al_3(Sc,Zr)$ particles in an Al-Zn-Mg-Cu-Sc-Zr alloy during conventional solution heat treatment and its effect on tensile properties. *Acta Materialia* **2008**, *56*, 3723-3238. doi:10.1016/j.actamat.2008.04.005
129. Zeng, F.; Xia, C.; Gu, Y. The 430 ^{o}C isothermal section of the Al-4Mg-Sc-Zr quaternary system in th Al rich range. *Journal of Alloys and Compounds* **2004**, *363*, 175-181. doi:10.1016/S0925-8388(03)00393-1
130. Alabin, N.A.; Belov, N.A.; Tabachkova, N.Yu.; Akopyan, T.K. Heat resistance of Al-Zr-Sc system for electrical applications: analysis and optimization of phase composition. *Non-Ferrous Metals* **2015**, *2*, 36-40. doi:10.17580/nfm.2015.02.07
131. Riddle, Y.W.; Sanders Jr., T.H. A study of coarsening, recrystallization, and morphology of microstructure in Al-Sc-(Zr)-(Mg) alloys. *Metallurgical and Materials Transactions A* **2004**, *35*, 341-350. doi:10.1007/s11661-004-0135-3
132. Li, G.; Zhao, N.; Liu, T. et al. Effect of Sc/Zr ratio on the microstructure and mechanical properties of new type Al-Zn-Mg-Sc-Zr alloys. *Materials Science and Engineering A* **2014**, *617*, 219-227. doi:10.1016/j.msea.2014.08.041
133. Clouet, E.; Nastar, M.; Sigli, C. Nucleation of Al_3Zr and Al_3Sc in aluminum alloys: From kinetic Monte Carlo simulations to classical theory. *Physical Review B* **2004**, *69*, 064109. doi:10.1103/PhysRevB.69.064109
134. Knipling, K.E.; Seidman, D.N.; Dunand, D.C. Ambient- and high-temperature mechanical properties of isochronally aged Al-0.06Sc, Al-0.06Zr and Al-0.06Sc-0.06Zr (at. %) alloys. *Acta Materialia* **2011**, *59*, 943-954. doi:10.1016/j.actamat.2010.10.017
135. Knipling, K.E.; Karnesky, R.A.; Lee, C.P. et al. Precipitation evolution in Al-0.1Sc, Al-0.1Zr and Al-0.1Sc-0.1Zr (at. %) alloys during isochronal aging. *Acta Materialia* **2010**, *58*, 5184-5195. doi:10.1016/j.actamat.2010.05.054
136. Xu, J.-H.; Freeman, A.J. Phase stability and electronic structure of $ScAl_3$ and $ZrAl_3$ and of Sc-stabilized cubic $ZrAl_3$ precipitates. *Physical Review B* **1990**, *41*, 12553. doi:10.1103/PhysRevB.41.12553
137. Harada, Y.; Dunand, D.C. Microstructure of Al_3Sc with ternary transition-metal additions. *Materials Science and Engineering A* **2002**, *329-331*, 686-695. doi:10.1016/S0921-5093(01)01608-2
138. Harada, Y.; Dunand, D.C. Creep properties of Al_3Sc and $Al_3(Sc,X)$ intermetallics. *Acta Materialia* **2000**, *48*, 3477-3487. doi:10.1016/S1359-6454(00)00142-7
139. Dorin, T.; Babaniars, S.; Jiang, L. et al. Precipitation sequence in Al-Sc-Zr alloys revisited. *Materialia* **2022**, *26*, 101608. doi:10.1016/j.mtla.2022.101608
140. Tolley, A.; Radmilovic, V.; Dahmen, U. Segregation in $Al_3(Sc,Zr)$ precipitates in Al-Sc-Zr alloys. *Scripta Materialia* **2005**, *52*, 621-625. doi:10.1016/j.scriptamat.2004.11.021
141. Forbord, B.; Lefebvre, W.; Danoix, F.; Hallem, H.; Marthinsen, K. Three dimensional atom probe investigation on the formation of $Al_3(Sc,Zr)$-dispersoids in aluminium alloys. *Scripta Materialia* **2004**, *51*, 333-337. doi:10.1016/j.scriptamat.2004.03.033
142. Fuller, C.B.; Murray, J.L.; Seidman, D.N. Temporal evolution of the nanostructure of Al(Sc,Zr) alloys: Part I – Chemical compositions of $Al_3(Sc_{1-x}Zr_x)$ precipitates. *Acta Materialia* **2005**, *53*, 5401-5413. doi:10.1016/j.actamat.2005.08.016
143. Fujikawa, S.I. Impurity diffusion of scandium in aluminum. *Defect and Diffusion Forum* **1997**, *143-147*, 115-120. doi:10.4028/www.scientific.net/ddf.143-147.115
144. Kerkove, M.A.; Wood, T.D.; Sanders, P.G.; Kampe, S.L.; Swenson, D. The Diffusion coefficient of scandium in dilute aluminum-scandium alloys. *Metallurgical and Materials Transactions A* **2014**, *45*, 3800-3805.doi:10.1007/s11661-014-2275-4
145. Peng, Y. Coarsening of Al_3Sc precipitates in Al-Mg-Sc alloys. *Journal of Alloys and Compounds* **2019**, *781*, 209-215. doi:10.1016/j.jallcom.2018.12.133
146. Marwuis, E.A.; Seidman, D.N. Nanoscale structural evolution of Al_3Sc precipitates in Al(Sc) alloys. *Acta Materialia* **2011**, *49*, 1909-1919. doi:10.1016/S1359-6454(01)00116-1